Journal of Hydrology 609 (2022) 127769

Contents lists available at ScienceDirect

Journal of Hydrology

journal homepage: www.elsevier.com/locate/jhydrol

Research papers

Using multiple isotopic and geochemical tracers to disentangle the sources of baseflow and salinity in the headwaters of a large agricultural watershed

Marty D. Frisbee [a,*], Marc W. Caffee [a,b], James J. Camberato [c], Greg Michalski [a,d]

[a] Department of Earth, Atmospheric, and Planetary Sciences, Purdue University, 550 Stadium Mall Drive, West Lafayette, IN 47907, USA
[b] Department of Physics and Astronomy, Purdue University, 525 Northwestern Ave, West Lafayette, IN 47907, USA
[c] Department of Agronomy, Purdue University, 915 W. State Street, West Lafayette, IN 47907, USA
[d] Department of Chemistry, Purdue University, 560 Oval Drive, West Lafayette, IN 47907, USA

ARTICLE INFO

Keywords:
Baseflow
Agricultural watershed
Regional groundwater
Sources of salinity
Geochemistry
Isotopes

ABSTRACT

Subsurface drainage modifications are a common practice in agricultural watersheds, especially in poorly drained soils of the American Midwest, yet our understanding of their impact on baseflow generation processes is incomplete. By extension, these same practices can make baseflow vulnerable to salinization. To address these knowledge gaps, a combined geochemical and multiple isotope approach was used to identify sources of baseflow and salinity in the Wabash River, draining Indiana, Ohio, and Illinois. Anomalously high salinity and high concentrations of F^-, SO_4^{2-}, Na^+, Sr^{2+}, and K^+ were measured in baseflow along the headwaters reach of the Wabash River from Fort Recovery, OH to Huntington, IN. Three river sites in the headwaters reach have low $^{36}Cl/Cl$ ranging from 27.5 (x 10^{-15}) to 33.4 (x 10^{-15}) that do not fall within the $^{36}Cl/Cl$ range for monthly precipitation. Their $^{36}Cl/Cl$ are consistent with ^{36}Cl dilution most likely due to the presence of old Cl^- found in potash (KCl) fertilizers. However, the $^{87}Sr/^{86}Sr$ ratios of the headwaters reach range from 0.708530 to 0.708904 (+/- 0.000025) and are similar to Silurian bedrock samples (0.708292 +/- 0.000047) indicating a geologic source for some solutes. The $\delta^{18}O$ of the headwaters reach are isotopically light and similar to cold-season recharge, whereas the $\delta^{18}O$ of the downstream river samples are similar to summer precipitation. The Cl^-, NO_3^-, Cl^-/Br^-, and $^{36}Cl/Cl$ data point to an anthropogenic source of salinity, namely KCl and road salt, whereas the F^-, Sr^{2+}, SO_4^{2-}, and $^{87}Sr/^{86}Sr$ data point to a geologic source of solutes. We infer that shallow groundwater that is Cl^- and NO_3^- rich mixes in the river with regional groundwater that is Cl^- and NO_3^- poor. The contribution of regional groundwater to baseflow in the headwaters reach is not insignificant (>58 percent) and these interactions should be considered in future hydrologic models of the Upper Wabash River. Without the aid of multiple isotopic and geochemical tracers, baseflow generation processes and sources of salinity in the headwaters reach would remain masked by the elevated solute concentrations associated with the shallow aquifers. Further research is needed to better understand the impact of KCl fertilizers on the overall salinity budgets of agricultural watersheds.

1. Introduction

Baseflow in pristine and/or relatively undisturbed watersheds is sourced primarily from groundwater and other delayed sources of water (Hall, 1968). Although baseflow is present year-round in perennial streams, it is especially critical in sustaining flow and supporting aquatic life during dry seasons and droughts. Baseflow generation in agricultural watersheds, in comparison, is quite complicated due to the presence of subsurface drainage modification systems and their impact on the shallow water table and suspected impacts to recharge to deep aquifers. The installation of tile drains and modified tile drains (Frankenberger et al., 2004; Fausey, 2005; Skaggs et al., 2010) is a common practice in humid areas with poorly draining soils such as the American Midwest. While subsurface drainage practices have obvious benefits to crop growth and yields (Kladivko, 2020), it remains uncertain how over a century of drainage modifications has impacted groundwater recharge

Abbreviations: UWR, Upper Wabash River; MWR, Middle Wabash River; LWR, Lower Wabash River; EC, Electrical Conductivity; SpC, Specific Conductivity; TDS, Total Dissolved Solids; DO, Dissolved Oxygen.

* Corresponding author.
E-mail address: mdfrisbee@purdue.edu (M.D. Frisbee).

https://doi.org/10.1016/j.jhydrol.2022.127769
Received 19 August 2020; Received in revised form 27 February 2022; Accepted 24 March 2022
Available online 30 March 2022

and baseflow generation in agricultural watersheds (Schilling, 2005; Zhang and Schilling, 2006). Unfortunately, we lack the field data in many cases to quantify how baseflow has been impacted by drainage modification since tile-drain installations either pre-date stream gauge installation and/or are located in watersheds that are largely ungauged. However, if we want to understand how aquatic agroecosystems are currently responding (and will respond in the future) to predicted changes in recharge associated with climate and land-use/land-cover change, then it is imperative that we improve our understanding of how drainage modifications alter recharge processes and impact baseflow generation processes in agricultural watersheds today.

Groundwater recharge is traditionally defined as water that has percolated through the unsaturated zone and entered the saturated porous media beneath the water table (Freeze and Cherry, 1979). In some agricultural watersheds, tile drains control the depth of the shallow water table passively (*e.g.*, traditional drainage) or actively (*e.g.*,

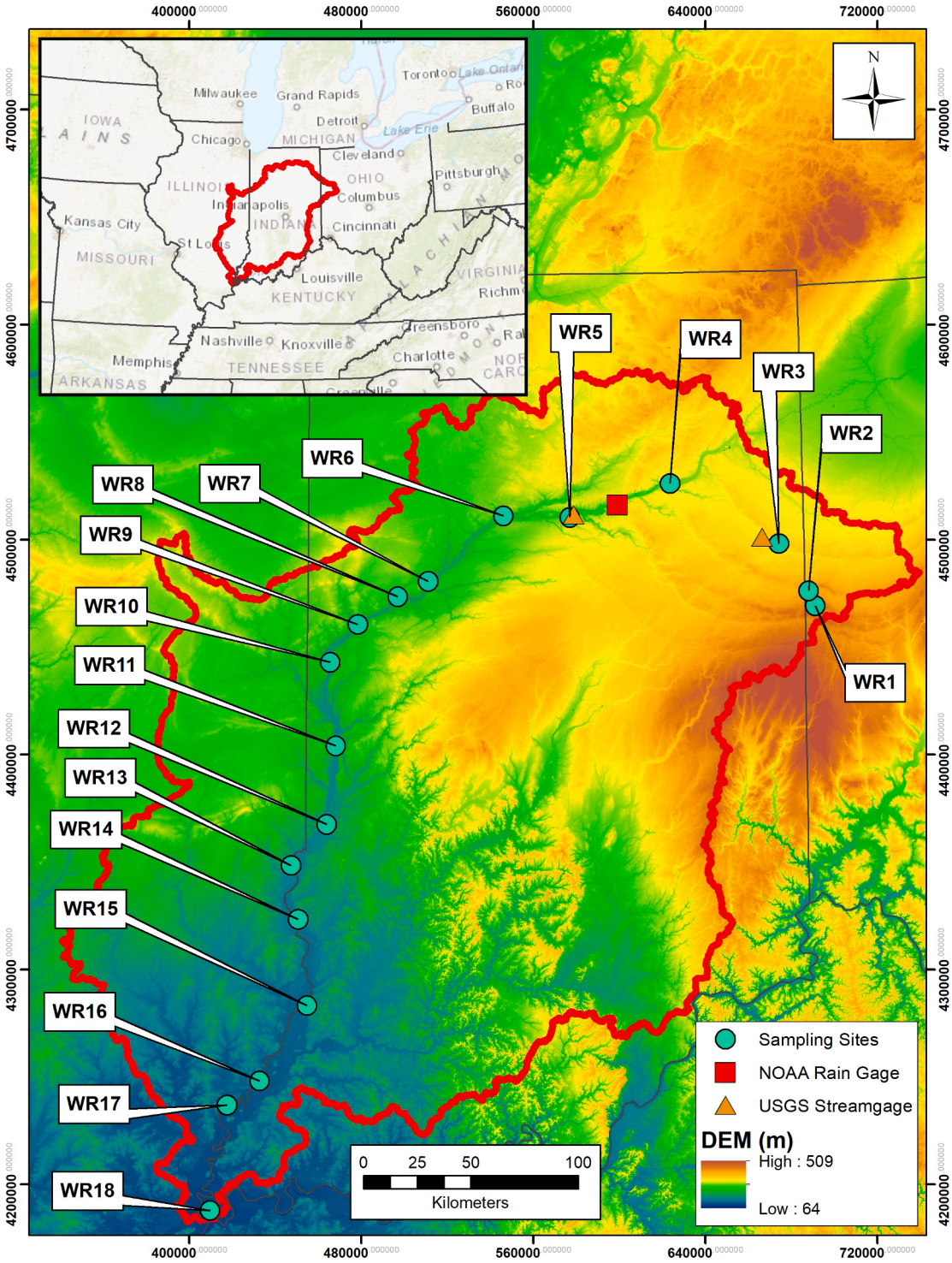

Fig. 1. Map of sampling sites in the Wabash River watershed. Inset map shows the regional basemap. State boundaries are thin black lines and can be matched to the inset map. UTM coordinates are shown around the perimeter of map.

controlled drainage, see Frankenberger et al., 2004). As a consequence, water that recharges the shallow aquifer may be quickly routed to a drain, thereby limiting circulation deeper than approximately 1 m and reducing the potential for recharge to deeper aquifers. There is growing concern that baseflow in these watersheds is sourced predominantly from tile-drainage systems (Schilling, 2005; Schilling et al., 2012). This has serious implications for water quality, salinity, nutrient persistence, and overall agroecosystem health (Tesoriero et al., 2013; Yaeger et al., 2013; Munn et al., 2018). Unfortunately, baseline geochemical and isotopic surveys of baseflow are lacking for many large agricultural watersheds in the American Midwest and globally. Data from synoptic and longitudinal surveys are sorely needed in these large agricultural watersheds.

To address the larger knowledge gap, two catchment-scale studies and one large watershed-scale study were initiated in the Wabash River watershed in 2015. The two catchment-scale studies were conducted in 2015 through 2016 to quantify the sources of baseflow in four small catchments draining agriculturally-fragmented land in northern and

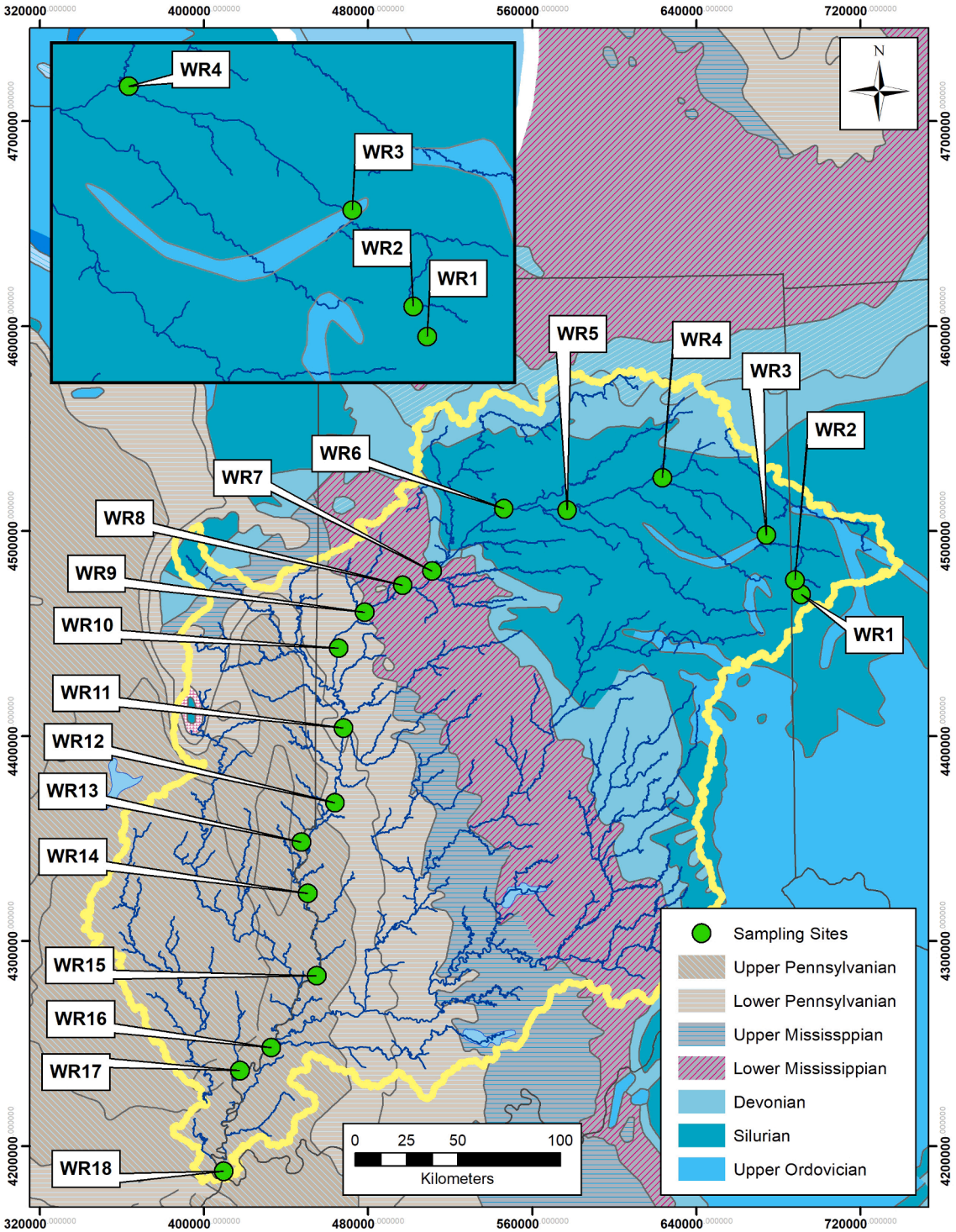

Fig. 2. Bedrock geology map of the Wabash River watershed. Inset map shows the bedrock geology of the headwaters reach. State boundaries are thin black lines and can be matched to the inset map of Fig. 1. UTM coordinates are shown around the perimeter of map.

central Indiana (Frisbee et al., 2017). This study revealed that relatively old (> 60 years), nitrate-free groundwater from confined glacial outwash sands supported baseflow in one catchment (Ross Reserve) located near West Lafayette, IN. This catchment was not as heavily impacted by agriculture as an adjacent catchment and as a consequence, the geochemistry of baseflow was quite different. The adjacent catchment was heavily impacted by agricultural runoff, thereby shortening the mean residence times of shallow groundwater and increasing the nitrate concentration substantially (Frisbee et al., 2017). During that same time, a synoptic sampling campaign was conducted in October and November of 2015 to identify the sources of baseflow in the much larger Wabash River and its major tributaries (Figs. 1 & 2). The Wabash River drains nearly 70 percent of Indiana and portions of Ohio and Illinois. It is the largest northern tributary to the Ohio River and the Ohio River is an important tributary to the Mississippi River. Over 65 percent of the northern Wabash River watershed drains agricultural land (Pyron and Neumann, 2008; Ahiablame et al., 2013; Wiener et al., 2016). The geochemical data from the Wabash River sampling campaign revealed high spatial complexity in geochemical concentrations and isotopic compositions. For example, anomalously high salinity (Cl^-) coincident with high total dissolved solids (TDS) and high concentrations of sodium (Na^+), sulfate (SO_4^{2-}), strontium (Sr^{2+}), potassium (K^+), and fluoride (F^-) were measured in river samples collected along the headwaters reach from Fort Recovery, OH (WR1 in Figs. 1 & 2) to the Forks of the Wabash near Huntington, IN (WR4 in Figs. 1 & 2). These observations pose two interrelated questions: what is the source of the high salinity and high TDS in the headwaters reach, and what does the observed high salinity and TDS of baseflow mean with respect to long-term water quality in the headwaters of the Wabash River?

While this research was initiated to improve our understanding of the sources of water that support baseflow in large agricultural watersheds, the observed high salinity in the headwaters reach of the Wabash River watershed has additional implications for the salinization of baseflow and Cl^- legacies in agricultural watersheds. Freshwater salinization is a global problem (Kaushal et al. 2018). Agricultural watersheds, such as those in the American Midwest, are particularly vulnerable to salinization because there are many potential sources of salt that can contribute to salinity including anthropogenic sources such as potash (KCl) fertilizers, seasonal ice/snow control using road salt (halite), septic and industrial effluent, home and business water-softener systems, and dust control on country roads using brines (Panno et al., 2006; Kaushal et al., 2018). Salt can also come from geologic sources (Warren, 2016), such as bedded halite. The dissolution of the fluid inclusions in the halite can potentially alter other solute concentrations (Cendón et al., 2008; Brennan et al., 2013). Due to its unique geologic setting and the presence of intensive agricultural practices, the headwaters of the Wabash River provides a unique setting to address this issue since there are numerous anthropogenic and potential geologic sources that can explain the observed salinity. In the study area, we investigate the following sources of salinity: 1) surface and shallow subsurface runoff from agricultural fields impacted by potash fertilizers (KCl or muriate of potash), 2) septic effluent (Vengosh and Pankratov, 1998; Panno et al., 2006), wastewater discharge (Wiener et al., 2016), or brine discharge from home water-softener systems (Panno et al., 2006), 3) discharge from deep sedimentary brines (or leaky gas wells) given the proximity of the headwaters reach to the Trenton Gas Field (Keith, 1985), and 4) deicing and dust-control agents in the study area (namely road salt or halite, although oil-field brines may have been used at one time in portions of northwestern OH; Kell et al., 2004). We also assess regional groundwater discharge from the Midwestern Basins and Arches Regional Aquifer System (Eberts and George, 2000) as a potential source of elevated Cl^- and other solutes. This aquifer is hosted in Silurian-Devonian carbonate rocks and is spatially extensive through northwestern Ohio, northern Indiana, southern Michigan, and northeastern Illinois (see Fig. 2 of Eberts and George, 2000).

The dataset presented here adds to the growing body of literature on the effects of landscape management, namely agricultural and drainage practices, on hydrological processes (Skaggs et al., 1994; Sloan et al., 2016; Buskirk et al., 2020). Impacts of agricultural practices on shallow subsurface processes have been well documented in research completed at the Intensively Managed Landscapes Critical Zone Observatory (IML-CZO) and in other independent study sites. The IML-CZO research has substantially improved our understanding on how surface agricultural practices, such as tillage, and subsurface drainage modifications have impacted water, solute, and nutrient yields from agriculturally managed landscapes (Kumar et al., 2018; Wilson et al., 2018). However, these studies rarely consider interactions with deeper aquifers, thereby limiting our understanding on their role in baseflow generation and their effect on salinity and TDS in these agricultural watersheds. This study bridges that gap by providing valuable insight into 1) the interactions between surface water, shallow aquifers, and deep aquifers (including regional flow in bedrock), 2) advantages and limitations in using multiple isotopic and geochemical tracers as forensic tools to differentiate between anthropogenic and geologic sources of salinity to agricultural rivers, and 3) the two-way exchange of salinity and nutrients between surface water, shallow aquifers, and deeper aquifers.

Here we address the following overarching questions 1) what is the source of the anomalous solute concentrations and high salinity in the headwaters reach of the Wabash River, 2) what do the solute concentrations reveal about the sources of baseflow in the headwaters reach, and 3) how much, if any, groundwater from the regional aquifer is discharged to the headwaters reach? We answer these questions using a multiple isotopic tracer approach combined with geochemical analyses. Specifically, chlorine-36 ratios ($^{36}Cl/Cl$) and chloride/bromide mass ratios (Cl^-/Br^-) are used to identify and differentiate between the numerous sources of salinity. Strontium isotopic ratios ($^{87}Sr/^{86}Sr$) are measured in river water, soil, and bedrock samples to identify the flowpaths that contribute to baseflow salinity (*i.e.,* is the salinity coming from the shallow subsurface, deeper aquifers, or gas field formations). Stable isotopes of water (^{18}O and ^{2}H) are used to identify mixing relationships between different sources of water and to identify sources of recharge.

2. Description of study area

2.1. Geography and geology

The Wabash River watershed is large (85,340 km^2) and the river flows through different geologic settings. Therefore, to aid in the comparison of data across the watershed, the entire watershed was divided into 3 regions that largely conform to preexisting subdivisions used in other publications. In this paper, we define the Upper Wabash River (UWR) as that portion of the river extending from Ft. Recovery, OH (WR1 in Fig. 1) to Lafayette, IN (WR7 in Fig. 1). The UWR primarily drains the Central Till Plain (Tipton Till Plain; see Gray, 2000). The Middle Wabash River (MWR) extends from Lafayette, IN south to Terre Haute, IN (WR12 in Fig. 1) and primarily drains the Central Till Plain (Gray, 2000). The MWR defined here conforms to the area defined in Doss (1994). The Lower Wabash River (LWR) extends from Terre Haute, IN south to New Haven, IL (WR18 in Fig. 1) and primarily drains the Southern Hills and Lowlands Region (Gray, 2000). The area that we have defined as the LWR largely conforms to the area delineated in Illinois flood maps (ISWS, 2020).

A brief geologic description is provided here (please see Casey (1996), Bugliosi (1999), and Eberts and George (2000) for a detailed explanation of the geological, hydrogeological, and geochemical framework of the study area including the Midwestern Basin and Arches Regional Aquifer System). Bedrock units and their associated deep aquifers in the study area are covered by glacial sediments up to approximately 154 m thick in some places from the Wisconsinan ice sheet (Fig. 3; Eberts and George, 2000). However, the unconsolidated glacial sediment is relatively thin (less than 30 m) along the headwaters

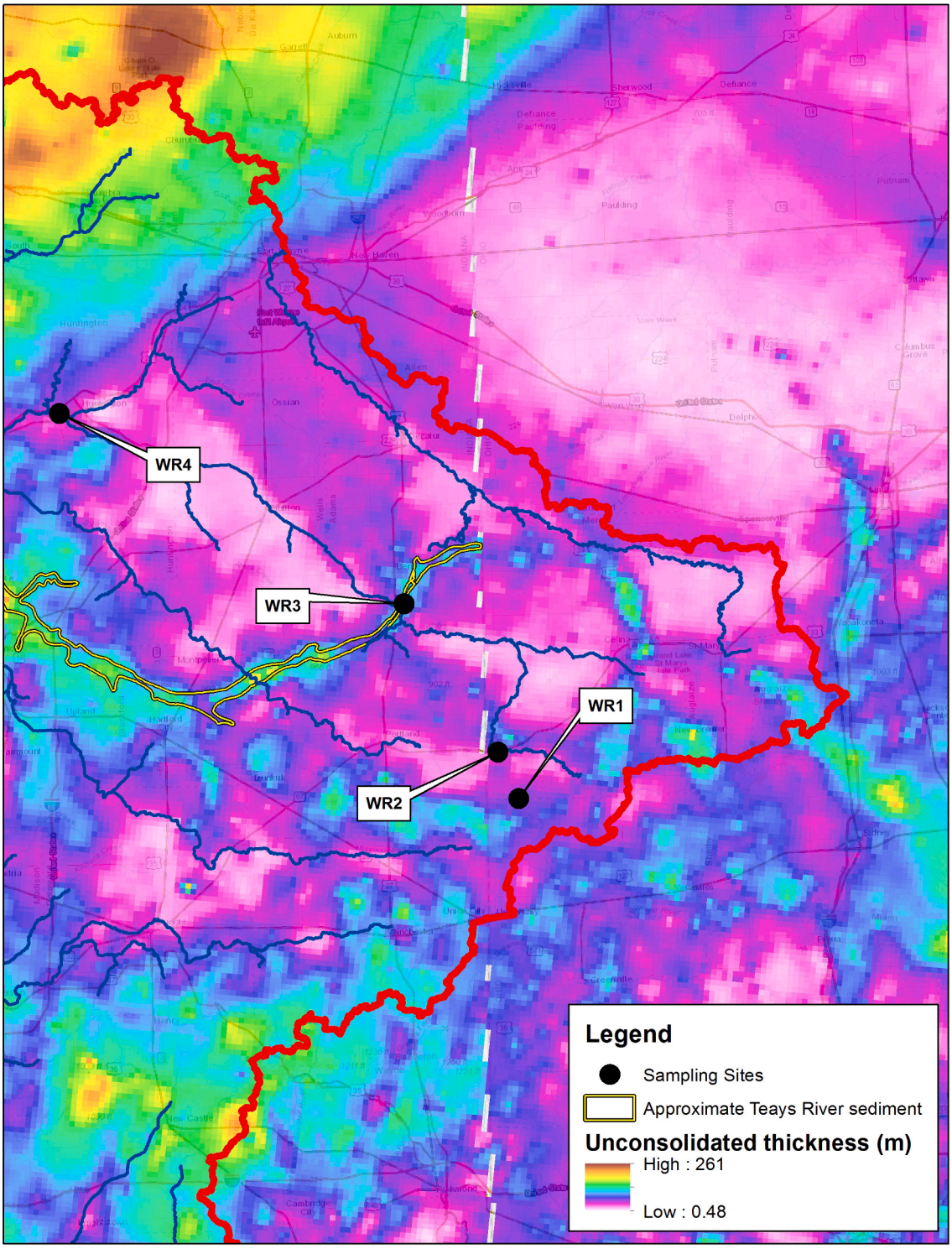

Fig. 3. Geologic map showing thickness of unconsolidated glacial sediment in headwaters reach. Map is modified from Bayless et al. (2017). The white dashed line represents the border between Indiana to the west and Ohio to the east. The watershed delineation can be matched to Figs. 1 and 2.

reach. Silurian bedrock units found in northeastern Indiana and northwestern Ohio were originally deposited in shallow marine and reef settings (Casey, 1996; McLaughlin et al., 2018). These units are primarily comprised of limestones and dolomites (Pinsak and Shaver, 1964) and contain evaporites and sulfide minerals (Pinsak and Shaver, 1964; Casey, 1996). Outcrops of Silurian bedrock (Wabash Formation) are exposed at the land surface in road cuts near the Forks of the Wabash, Huntington, IN (see site WR4 in Fig. 2) and near France Park, Logansport, IN (Frisbee et al., 2019; see site WR6 in Fig. 2). Discontinuous exposures of Upper Ordovician rocks are present beneath the unconsolidated sediment in the headwaters reach of the Wabash River watershed where the ancient Teays River system has eroded the Silurian carbonate sequence (Melhorn and Kempton, 1991; Figs. 2 and 3). The Ordovician rocks are primarily comprised of shales with a smaller proportion of interbedded limestones. The upper Ordovician rocks host the Maquoketa Group Aquifer System (Schmidt, 2009) that is coincident

with the buried Teays Valley. The Ordovician Trenton Limestone lies beneath the Maquoketa Group Aquifer System and it hosts the Trenton Gas Field and associated formation brines (Keith, 1985; Casey, 1996).

The headwaters reach of the Wabash River is positioned between the Michigan Basin located to the north (separated by the Kankakee Arch), the Illinois Basin located to the southwest (separated by the Cincinnati Arch), and the Appalachian Basin located to the east (separated by the Findlay Arch; see Fig. 2 of Eberts and George, 2000). The location between these arches has profoundly affected the underlying structure and attitude of sedimentary units, and groundwater flow directions. For example, older geologic units, such as Upper Ordovician, Silurian, and Devonian rocks, were brought closer to the land surface along the axes of these arches. Thus, bedrock units get younger moving west, north, and east from the axes of the arches (see Fig. 2 of Eberts and George, 2000). Uplift and glaciation have also affected groundwater flowpaths (Casey, 1996; Bugliosi, 1999; Eberts and George, 2000).

2.2. Hydrogeology and surface hydrology

Unconsolidated glacial sediments in the UWR and MWR (Fig. 3) host shallow phreatic aquifers. These aquifers are thought to contain primarily modern groundwater. Eberts and George (2000) report tritium (^{3}H) activities ranging from 3.0 to 20.6 TU in the shallow phreatic aquifers which were, at the time, consistent with modern recharge (< 70 years). Although Eberts and George (2000) did not collect samples of groundwater that are spatially coincident with the Wabash headwaters reach, they did sample a transect across the UWR. They report some overlap in δ^{18}O between the shallow phreatic aquifers in the unconsolidated glacial deposits (−7.85‰ to −7.65‰) and the shallow portion of the regional carbonate aquifer (−7.90‰ to −7.75‰). However, isotopically light groundwater (−14.4‰ to −7.40‰) was found in the deep regional carbonate aquifer with the lightest groundwater found in the Maumee River basin northeast of Fort Wayne, IN. This isotopically light groundwater was inferred to be a mixture of Pleistocene recharge and modern, cold-season recharge (Eberts & George, 2000).

The Silurian bedrock units, whose thickness generally increases to over 760 m progressing northward from the axes of the arches toward Michigan, support the Midwestern Basin and Arches Regional Aquifer System. Regional groundwater flow in the Silurian carbonate aquifer follows the dip away from the axes of the arches. Eberts and George (2000) modeled the hydrogeology of this aquifer system and found that local-scale groundwater (*i.e.*, short groundwater flowpaths that are affected by seasonal variations in recharge) likely accounts for 50 to 97 percent of baseflow to streams in the region, while regional groundwater (*i.e.*, long groundwater flowpaths that are minimally affected by variations in seasonal recharge) accounts for 3 to 50 percent of baseflow. Eberts and George (2000) also present isotopic data on samples of groundwater collected from the deep regional carbonate aquifer. These samples were found to be largely tritium dead (^{3}H < 0.1 TU). In addition, radiocarbon residence times tended to get longer as flowpath lengths increased, ranging up to approximately 13,000 years near the distal end of a set of flowpaths in the Maumee River basin near Lake Erie (Eberts and George, 2000). Thus, they inferred that a significant proportion of Pleistocene recharge from the Last Glacial Maximum is present in the deep regional carbonate aquifer.

The Wabash River originates from seeps located on private property south of Fort Recovery, OH (west of WR1 in Figs. 1, 2). During this study, water samples could not be collected from the private property. However, water samples were collected where the headwater stream is channelized in a ditch located approximately 1.5 km downstream of the private property at the Historic Anthony Wayne Parkway Roadside Park - Wabash River (16S 691220 mE, 4,469,326 mN; see WR1 in Fig. 2). The stream channel then takes a circuitous route, looping northeast then northwest back to Fort Recovery, OH (see site WR2 in Fig. 2) before flowing into northeastern Indiana (Fig. 1). This paper focuses on the headwaters reach from Fort Recovery, OH (site WR1 in Fig. 2) to Huntington, IN (site WR4 in Fig. 2).

There are three USGS stream gauging sites in the headwaters reach of the Wabash River and all three sites are located in Indiana. Two of our sampling sites in the headwaters reach are located near a USGS stream gauging site. Site WR3 is located near the stream gauge at Linn Grove, IN (site 03322900; https://waterdata.usgs.gov/in/nwis/inventory/?site_no=03322900; last accessed on 08 February 2022) and Site WR4 is located near the stream gauge at Huntington, IN (site 03323500; https://waterdata.usgs.gov/in/nwis/inventory/?site_no=03323500; last accessed on 08 February 2022). The average daily discharge at Linn Grove over the period from 01 January 1965 to 31 December 2019 ranged from 0.11 to 394 $m^3 s^{-1}$. A continuous record of discharge over the same time period is not available at Huntington, IN. However, the average daily discharge at Huntington over the period from 01 January 1965 to 31 December 2001, excluding incomplete years of 1992 and 1993 ranged from 0.10 to 239 $m^3 s^{-1}$.

An average annual hydrograph (Fig. 4) was created for the headwaters reach over a 55-year period of record (01 January 1965 to 31 December 2019) using stream gauge data from the USGS gauge at Linn Grove, IN. A set of flow duration curves (FDCs) was created for the discharge data from the USGS gauging sites at Linn Grove, Huntington, and an additional site at Peru, IN located in proximity to Site WR5. Daily discharge data for the Wabash River near Peru, IN was obtained from USGS Site 03,327,500 (https://waterdata.usgs.gov/in/nwis/inventory/?site_no=03327500; last accessed on 08 February 2022) over the same interval as the Linn Grove site. These curves (Fig. 5) show that the headwaters reach is relatively flashy and that discharge generally increases from Linn Grove, IN (WR3) to Peru, IN (near WR5). Here, we define flashy streamflow as stream discharge that responds quickly to rain or snowmelt events and has an event-scale recession that is usually steep (Poff et al., 1987). For example, the annual hydrograph of the headwaters reach shows quick responses to precipitation events, particularly during summer and fall thunderstorms (see days 160 to 280 of Fig. 4). In addition, the slopes of the flow duration curves shown in Fig. 5 are slightly steeper in the 20 to 80% exceedence probability range of the plots than expected for groundwater-dominated streams (Searcy, 1959). In general, the highest stream flows occur in the spring after snowmelt (late February through late April) and prior to the growing season (days 52 to 115 of Fig. 4). Stream flows gradually decrease over the course of the summer growing season despite plentiful rainfall during this time (Fig. 4). The lowest stream flows occur in the autumn near the end of the growing season and prior to winter storms occurring in November and December (Figs. 4 & 5). Miller and Lyon (2021) report similar flashy behavior for tile-drained watersheds in Ohio. Baker et al. (2004) examined flashy stream behavior in Midwestern watersheds using a new flashiness index.

2.3. Climatology

The headwaters reach of the Wabash River experiences cold winters and hot summers. Only one weather station was found in the headwaters reach with a sufficiently long and continuous period of record comparable to the 55-year period of record of from the stream gauge at Linn Grove, IN. Meteorological data were obtained from NOAA Climate Data Online (https://www.ncei.noaa.gov/maps/daily/; last accessed on 10 February 2022) for a weather station located in Berne, IN, approximately 7.0 km to the east of Linn Grove, IN (01 January 1965 to 31 December 2019; Fig. 1). The average low and high January (winter) temperatures measured at Berne, IN over the last 55 years are –8.0 °C and 0.4 °C, respectively, and the average low and high July (summer) temperatures are 17.8 °C and 29.2 °C. Berne, IN receives an average of 100.3 cm of precipitation per year (Fig. 6). Precipitation is seasonally distributed; 19 percent occurs in the winter months, 30 percent occurs in the spring months, 30 percent occurs in the summer months, and 21 percent occurs in the fall months. The study area receives between 10.7 cm and 157.9 cm of snow (not snow-water equivalent) per year.

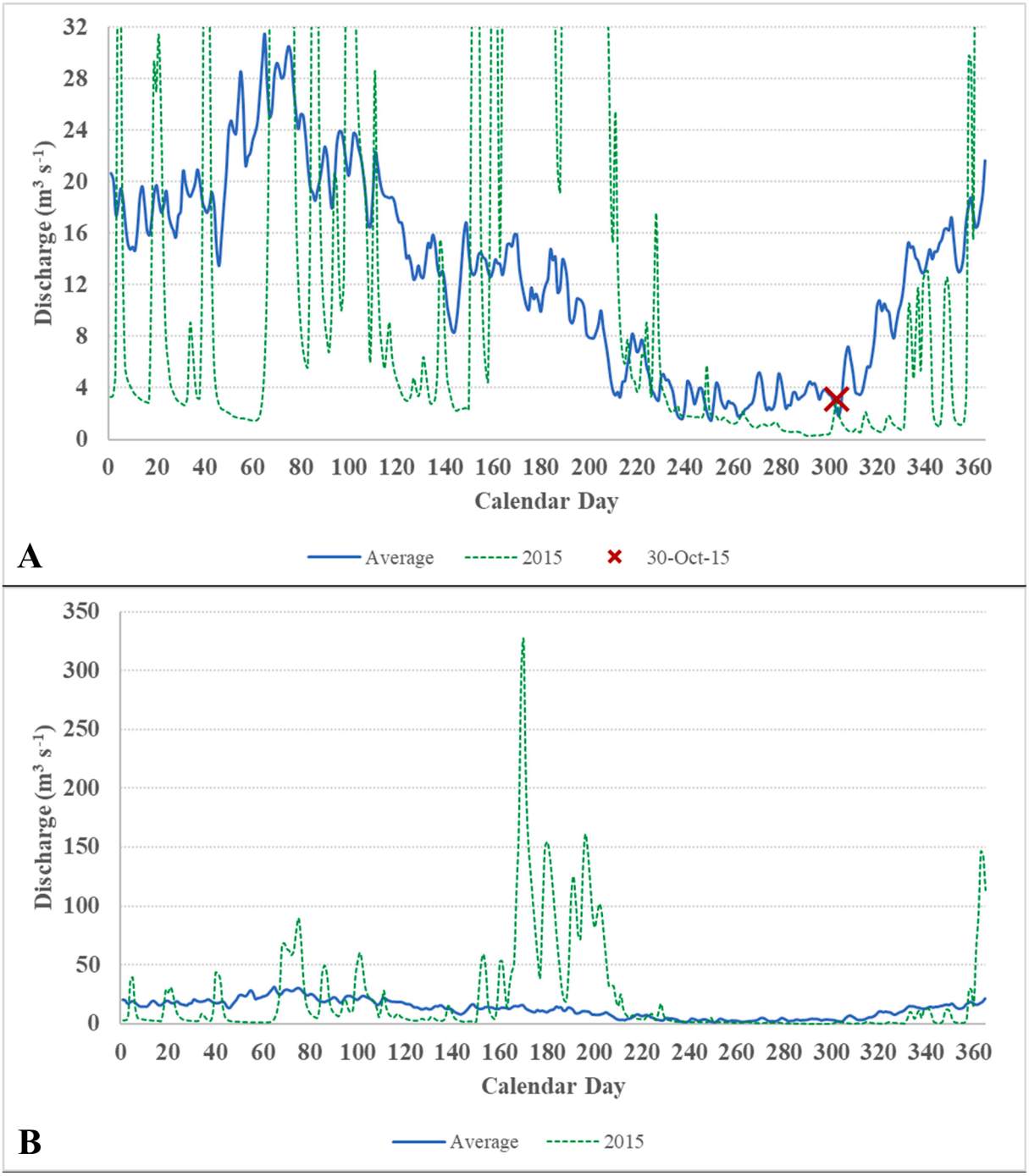

Fig. 4. Average annual hydrograph of the headwaters reach over a 55-year period of record (01 January 1965 to 31 December 2019) using stream gauge data from the USGS gauge at Linn Grove, IN. A) Y-axis is scaled to show the magnitude of discharge during the autumn baseflow sampling period and the sampling date is shown by a red 'X'. B) Y-axis is scaled to show the magnitude of discharge during the flooding event of 2015. (For interpretation of the references to colour in this figure legend, the reader is referred to the web version of this article.)

During the spring and summer of 2015, the study area received the 4th highest annual precipitation observed over the 55-year period of record (Fig. 6). This resulted in widespread flooding throughout the Wabash River watershed (see green dashed line in Fig. 4). Floodwaters began to recede near the end of August (calendar day 240 of Fig. 4b) and baseflow conditions resumed in late September and were persistent through October and early November. Samples were collected in the UWR on 30 October 2015, indicated by the red *x-mark* in Fig. 4a, confirming that samples were collected during acceptable baseflow conditions.

3. Methods

3.1. Field chemistry and geochemical analyses

The entire main channel of the Wabash River was longitudinally sampled over the course of 3 days. Sites WR1 through WR5 (Fig. 1) in the UWR were sampled on 30 October 2015 and the remaining two sites in the UWR (WR6 and WR7) were sampled on 06 November 2015. The MWR sampling sites (WR8 to WR12; Fig. 1) were sampled on 06 November 2015. The LWR sampling sites (WR13 to WR18; Fig. 1) were

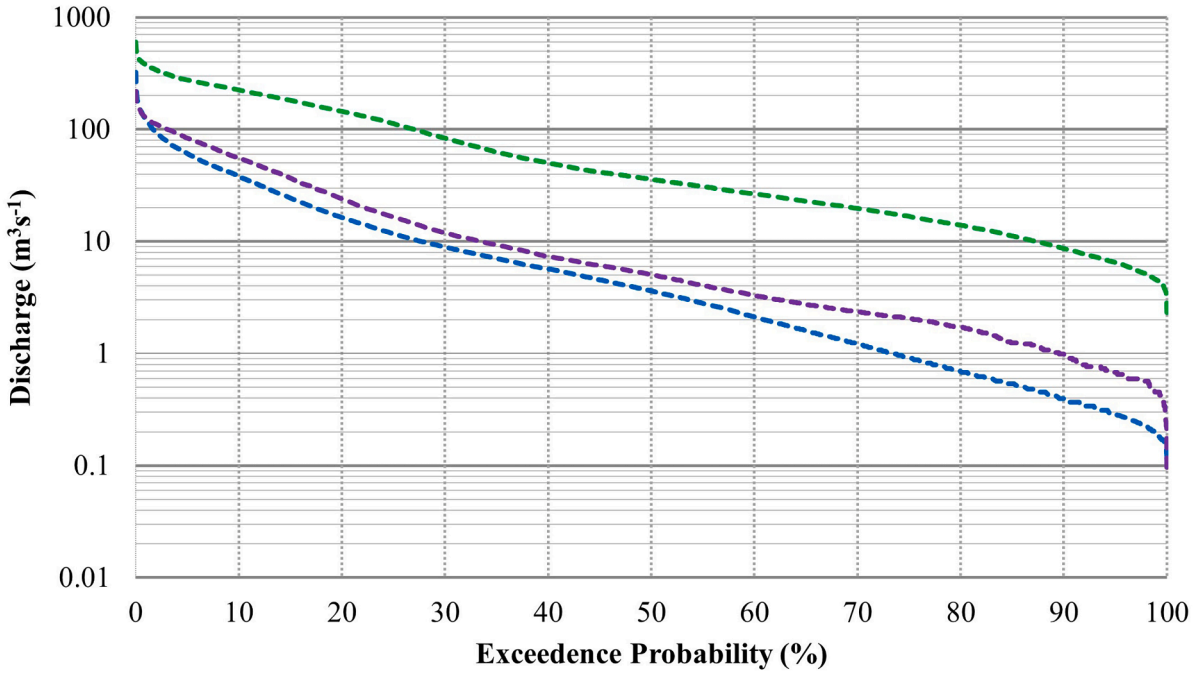

Fig. 5. Flow duration curves of headwaters reach over a 55-year period of record using stream gauge data from the USGS gauges at Linn Grove, IN (blue dashed line; includes data from 01 January 1965 to 31 December 2019), Huntington, IN (purple dashed line; includes data from 01 January 1965 to 31 December 2001), and Peru, IN (green dashed line; includes data from 01 January 1965 to 31 December 2011). Incomplete years were excluded from the flow duration curves. (For interpretation of the references to colour in this figure legend, the reader is referred to the web version of this article.)

sampled on 20 November 2015.

A YSI Professional Plus (Pro Plus) multi-parameter meter (https://www.ysi.com/proplus; last accessed on 10 February 2022) was used to measure field chemical parameters including: pH, temperature, electrical conductivity (EC; µS cm^{-1}), and dissolved oxygen (DO; mg L^{-1} and % saturation relative to air saturation). Specific conductivity (SpC; µS cm^{-1}), EC corrected to 25°C, is calculated by the YSI meter by: $SpC = EC * 1.91$; where 1.91 is the temperature coefficient for waters at 25°C. Total dissolved solids (TDS; mg L^{-1}) is also calculated by the YSI meter by: $TDS = SpC \times 0.65$. The YSI meter was calibrated prior to the first sample site each day using a three-point calibration for pH and EC. The calibration was checked randomly throughout the day. A new DO membrane and fresh electrolyte (O_2 solution) was used for each sampling trip.

All water samples were collected by tossing one end of a 10 m length of viton tubing into the river from the bank, letting the tubing settle to the bottom of the channel, and then connecting the other end to a Geotech 0.45 µm dispos-a-filter (http://www.geotechenv.com/disposable_filter_capsules.html; last accessed on 08 February 2022). The tubing was then fed into the drive head of a Pegasus Alexis peristaltic pump and pumped for 3 to 5 min to completely flush the filter. The filters were replaced approximately every 2 to 3 sample sites. Water samples were collected in clean, non-acidified 250 mL wide-mouth HDPE Nalgene bottles for general geochemistry analyses (standard cations and anions) which were completed at the Chemical Laboratory of the New Mexico Bureau of Geology and Mineral Resources. The suite of cations includes sodium (Na^+), potassium (K^+), magnesium (Mg^{2+}), calcium (Ca^{2+}), and strontium (Sr^{2+}) and these were measured using a PerkinElmer Optima 5300 DV ICP-OES per EPA 200.7. The suite of anions includes chloride (Cl^-), bromide (Br^-), fluoride (F^-), nitrate (NO_3^-), and sulfate (SO_4^{2-}) and these were measured using a Dionex ICS-5000 IC according to EPA 300.0. Alkalinity was not measured in the field, but alkalinity as $CaCO_3$ and bicarbonate (HCO_3^-) was completed in the lab according to EPA 310.1. Silica (SiO_2) concentrations were completed according to SM 1030E. Duplicates were analyzed on every tenth sample to assess repeatability and analytical precision. Detection limits, analytical uncertainty, and charge balances were reported from the lab and are provided within this paper.

3.2. Chlorine-36 analyses

Chlorine-36 ratios ($^{36}Cl/Cl$) and Cl^-/Br^- mass ratios (mg L^{-1}/mg L^{-1}) are used to identify and differentiate between the numerous sources of salinity that are present in the headwaters of the Wabash River watershed. Potential chloride endmembers were identified through previous research by Frisbee et al. (2017) and from other published data (see below). Groundwater recharged during the bomb-pulse era should have elevated $^{36}Cl/Cl$ compared to pre-anthropogenic and modern recharge (Clark and Fritz, 1997; Corcho Alvarado et al., 2005; Tosaki et al., 2011; Phillips, 2000; 2013; Shaw et al., 2014). Frisbee et al. (2017) found that springs in Shades State Park in central Indiana were discharging a substantial component of groundwater recharged during or immediately after the bomb-pulse era. Those springs had $^{36}Cl/Cl >$ 1300 (x 10^{-15}). Baseflow in streams draining those same catchments ranged from 720 (x10^{-15}) to 1250 (x10^{-15}). In comparison, pre-anthropogenic $^{36}Cl/Cl$ in groundwater for northern Indiana should range from 300 (x10^{-15}) to approximately 450 (x10^{-15}) based on data provided in Davis et al. (2000, 2003). Monthly-integrated samples of precipitation were collected in West Lafayette, IN to provide an end-member for within-year runoff (Frisbee et al., 2017). Geologic brines can be found in the headwaters of the Wabash River watershed. Brines tend to have very low $^{36}Cl/Cl$ ($<20 \times 10^{15}$) relative to modern and clean, unaffected groundwater (Vengosh, 2014).

The expected range of Cl^-/Br^- mass ratios for wet deposition varies with distance inland from oceanic sources (Short et al., 2017). Davis et al. (1998, 2000) report Cl^-/Br^- less than approximately 250 for clean modern groundwater, defined as groundwater unaffected by Cl^- pollution. Regionally, Panno et al. (2006) reports a Cl^-/Br^- range of 23 to 521 and a mean of 156 for pristine groundwater from sand and gravel aquifers in nearby northeastern Illinois. Frisbee et al. (2017) report $Cl^-/$

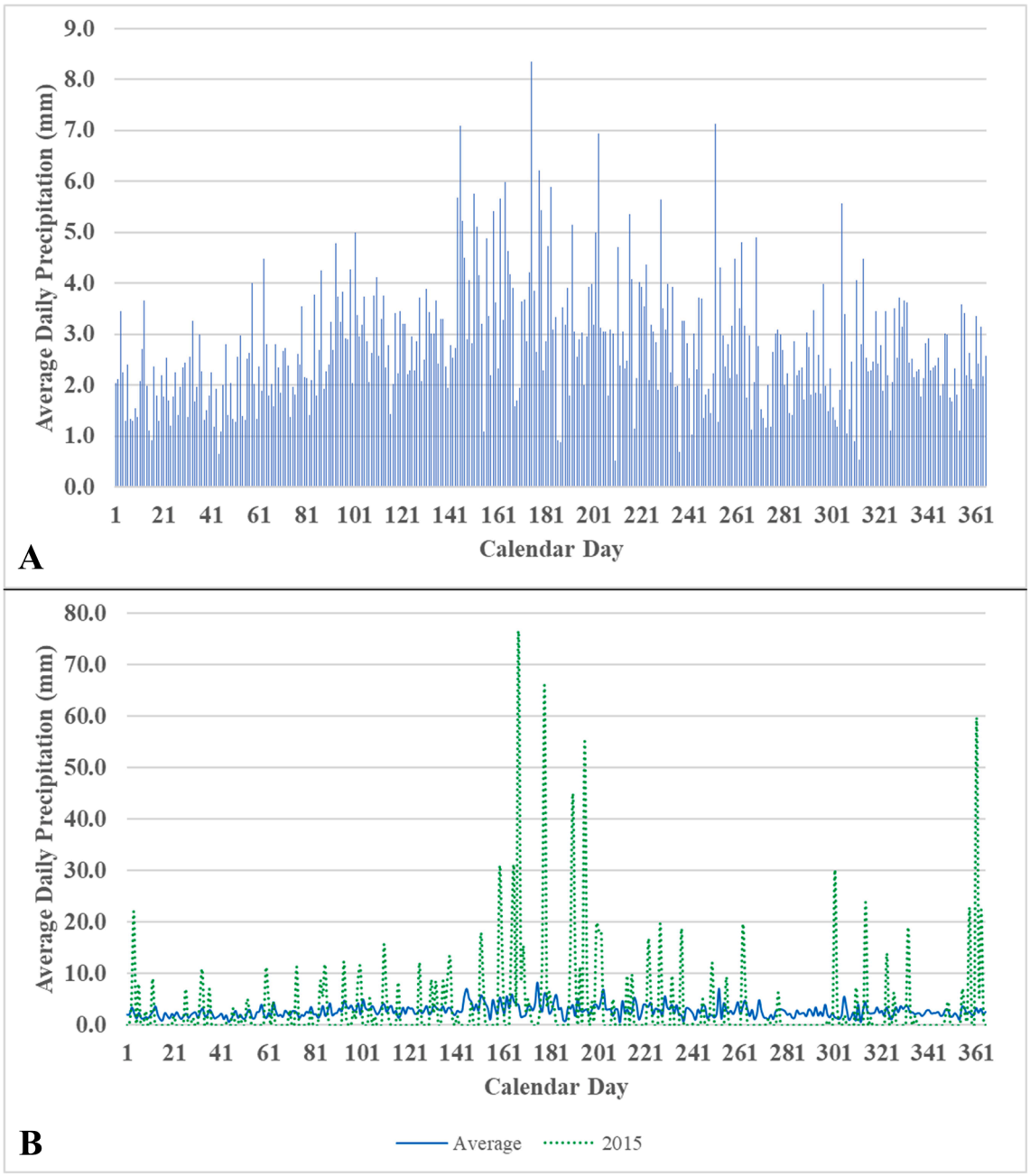

Fig. 6. A) Hyetograph of average annual precipitation created from meteorological data obtained from NOAA Climate Data Online for a weather station located in Berne, IN, approximately 7.0 km to the east of Linn Grove, IN (period of record is 01 January 1965 to 31 December 2019). B) Y-axis is scaled to show the increased precipitation occurring in 2015 (green dashed line). (For interpretation of the references to colour in this figure legend, the reader is referred to the web version of this article.)

Br^- ranging from 30 to 95 for clean, unaffected springs in central Indiana. Cl^-/Br^- mass ratios tend to be elevated (>1000) in geologic brines and in waters that interacted with evaporite minerals (Davis et al., 1998). Therefore, $^{36}Cl/Cl$ can be coupled with Cl^-/Br^- to potentially differentiate between sources of Cl^- (Davis et al., 2000; Davis et al., 2003).

Filtered water samples were collected from each river site in clean, non-acidified, wide-mouth 1000 mL HDPE Nalgene bottles for ^{36}Cl analyses. Precipitation was collected on a monthly basis in 2015; the winter precipitation samples that were collected after baseflow samples were collected for this study are not shown in this paper. The $^{36}Cl/Cl$ of precipitation was assumed to be equivalent to the $^{36}Cl/Cl$ of modern (within year) recharge and surface runoff. This assumption is made based on the inferred flashy behavior of streams in the region. Precipitation was collected in clean buckets installed in an open grassy area located near West Lafayette, IN (Frisbee et al., 2017). The buckets were inspected daily (or immediately following precipitation events). Event-scale precipitation samples were then poured into clean 2L Nalgene bottles. Samples were then combined at the end of the month to create integrated monthly samples. The buckets were washed with Alconox and rinsed with deionized water after precipitation samples were collected, and then re-installed.

Samples of road salt (halite) were acquired from two salt vendors that supply the Indiana Department of Transportation. One sample was provided by Compass Minerals from Silurian salt deposits near Goderich, Ontario and the other sample was provided by Cargill Deicing

from Silurian salt deposits near Cleveland, OH. Halite samples were dissolved in deionized water, given a sulfur reduction step to reduce interference with ^{36}S, and AgCl was precipitated from the water sample. All $^{36}Cl/Cl$ analyses and chemistry steps were completed at the Purdue PRIME Lab using accelerator mass spectrometry (AMS; Sharma et al., 2000; https://www.physics.purdue.edu/primelab/). The reported relative measurement uncertainty ranged between +/- 2.3 to 4.5%.

3.3. Strontium Isotope analyses

Strontium isotopic ratios ($^{87}Sr/^{86}Sr$) of water samples are compared to the $^{87}Sr/^{86}Sr$ of rocks, rock leachate, and glacial sediment leachate present in the study area to identify which rocks host the flowpaths, assuming that the $^{87}Sr/^{86}Sr$ of each endmember are distinct (Hogan and Blum, 2003; Frisbee et al., 2017). Filtered water samples were collected from each river site in clean, non-acidified, wide-mouth 1000 mL HDPE Nalgene bottles for $^{87}Sr/^{86}Sr$ analyses. Samples of geologic material found in the study area were also collected for whole rock and rock leachate $^{87}Sr/^{86}Sr$ analyses. Bedrock samples were also collected in the study area including Silurian Wabash Formation (dolomitic limestone), Silurian Brassfield Formation (dolomitic limestone), and Ordovician Platteville Formation (dolostone). Whole-rock samples were crushed and processed at Isotope Tracer Technologies. Glacial sediment samples were collected from the surface and shallow subsurface in the study area. The glacial sediment samples were leached using deionized water since they are a mix of rock clasts and clay material and leaching is thought to provide a more representative $^{87}Sr/^{86}Sr$ of the unconsolidated glacial sediment. This technique has been applied successfully in other recent studies (Frisbee et al., 2017; Warix et al., 2020; Gleason et al., 2020). Rock-leachate samples were created by: 1) placing 300 g of glacial sediment in clean 2 L Nalgene bottles, 2) filling the bottle with deionized water (DI), 3) capping the bottle and leaching the rock samples for 2 months, 4) decanting the water from the bottle, and 5) measuring the strontium (Sr^{2+}) concentrations of the water and measuring the $^{87}Sr/^{86}Sr$ of the rock-leachate. All $^{87}Sr/^{86}Sr$ analyses were completed by Isotope Tracer Technologies using Thermal Ionization Mass Spectrometry (TIMS). The reported analytical uncertainty is provided. For comparison purposes, we use $^{87}Sr/^{86}Sr$ ratios for precipitation that were reported in Sherman et al. (2015). Specifically, $^{87}Sr/^{86}Sr$ for precipitation for Dexter, MI (0.709966 +/- 0.000360) and Detroit, MI (0.708785 +/- 0.000390) are used as potential endmembers given the proximity of these sites to the headwaters of the Wabash River in northern IN and OH.

3.4. Stable isotopes of water

Stable isotopes of water, ^{18}O and ^{2}H, were used to identify the sources of water contributing to baseflow. Small aliquots of water (5 mL) were pipetted from each general chemistry sample. Stable isotopic ratios of water (δ^2H and $\delta^{18}O$) were analyzed by the Purdue Stable Isotope Lab using an LGR Triple Isotope Liquid Water Analyzer. Three standards were used for calibration: $\delta^2H = 18.1‰$ and $\delta^{18}O = 2.78‰$, $\delta^2H = -117.2‰$ and $\delta^{18}O = -15.7‰$, and $\delta^2H = -44.5‰$ and $\delta^{18}O = -6.9‰$. Each water sample was analyzed ten times; the first four runs were discarded while the last six runs were averaged to provide the final isotopic ratios. δ^2H and $\delta^{18}O$ were reported relative to VSMOW (Vienna Standard Mean Ocean Water). The precision of analyses relative to known standards are 0.61‰ for δ^2H and 0.09‰ $\delta^{18}O$. Uncertainties for each sample are provided.

4. Results

4.1. Field chemistry and spatial trends in geochemical concentrations

The SpC values (829 to 1051 μS cm^{-1}) measured in the headwaters reach are nearly twice as large as those measured in the remainder of the UWR (493 to 676 μS cm^{-1}) and almost all of the MWR (580 to 604 μS cm^{-1}), except for WR12 (1246 μS cm^{-1}) at Terre Haute, IN (Table 1). Only the measurements made at the LWR sampling sites (1061 to 1255 μS cm^{-1}), with the exception of WR18, are higher than those measured in the headwaters reach. Site WR3 has the lowest SpC of the headwaters reach. This site also has the lowest DO (59.1%) of the headwater reach; Sites WR1, WR2 and WR4 have DO values of 65.7, 84.0, and 82.5%, respectively.

The Cl^- concentration measured at WR1 is 39.4 mg L^{-1} (Fig. 7, Table 2) and Cl^- concentrations increase to 56.4, 68.7, and 131 mg L^{-1} at sites WR2, WR3, and WR4, respectively. Immediately downstream of WR4 there is a substantial decrease in Cl^- (29 mg L^{-1}) and the remaining stream sites have Cl^- concentrations less than 34.2 mg L^{-1}. For comparison, water samples collected in the Ohio River upstream of the confluence with the Wabash River at Mt. Vernon, IN and downstream of the confluence at Old Shawneetown, IL have Cl^- concentrations of 37 mg L^{-1} and 29.2 mg L^{-1}, respectively. Sodium concentrations largely parallel Cl^- concentrations (Fig. 7, Table 2).

Strontium and sulfate concentrations are surprisingly high in the headwaters reach. Sr^{2+} concentrations range from 1.13 to 2.77 mg L^{-1} in the headwaters reach while, in comparison, the Sr^{2+} concentrations of the remaining sample sites are less than 0.69 mg L^{-1} (Table 2, Fig. 7). Sr^{2+} concentrations decrease with increasing distance downstream of the headwaters reach. SO_4^{2-} concentrations in the headwaters reach range from 105 to 143 mg L^{-1}, while in comparison, the average SO_4^{2-} concentration of the remaining sample sites is 50.6 +/- 6.7 mg L^{-1}. Only one sampling site in the lower reaches of the Wabash River watershed has a SO_4^{2-} concentration comparable to the headwater reach. Site WR16 has a SO_4^{2-} concentration of 175 mg L^{-1} and is located immediately downstream of a coal-burning power plant near Mt. Carmel, IL. The sites in the headwaters reach also have elevated F^- concentrations ranging from 0.30 to 0.51 mg L^{-1} relative to the other sampling sites which have an average F^- concentration of 0.26 +/- 0.03 mg L^{-1} (Fig. 7).

The solute concentrations of the water sample collected from Site WR3 are odd relative to Sites WR2 and WR4 in the headwater reach sites. The concentrations of Cl^-, Na^+, Br^-, and F^- increase progressively from WR2 to WR4 (Tables 1 & 2). However, WR3 has the highest concentrations of Mg^{2+}, Sr^{2+}, and SO_4^{2-} of the headwaters reach (Tables 1 & 2). This site also has the lowest SpC and DO, and lowest concentrations of Ca^{2+}, NO_3^-, and Si.

4.2. Spatial trends in Cl^-/Br^- and $^{36}Cl/Cl$

The Cl^-/Br^- of sites WR1, WR2, WR3, and WR4 are all elevated relative to the remaining sites, except for WR9, WR14, and WR15. Sites WR1, WR2, WR3, and WR4 have Cl^-/Br^- ratios of 985, 1077, 758, and 1139, respectively (Table 3, Fig. 8). Cl^-/Br^- ratios then decrease downstream reaching a minimum at site WR6 near Logansport, IN (Fig. 8). The remainder of the Wabash River sampling sites, excluding WR9, WR14, and WR15, have Cl^-/Br^- ranging from 229 to 649 and show little variability through portions of the MWR and LWR. Sites WR9, WR14, and WR15 all have Cl^-/Br^- >1300.

The $^{36}Cl/Cl$ of monthly precipitation from April to October 2015 ranges from 43.2 +/- 2.8 (x 10^{-15}) to 79.8 +/- 3.8 (x 10^{-15}; Table 3). The range of $^{36}Cl/Cl$ measured in precipitation for this study is illustrated by the grey box in Fig. 8. All of the river samples have $^{36}Cl/Cl$ lower than the expected range for clean groundwater in the region (~450 × 10^{-15}) based on data provided in Davis et al. (2000, 2003). Site WR1 has a $^{36}Cl/Cl$ of 50.0 +/- 2.6 (x10^{-15}), while the $^{36}Cl/Cl$ ratios of sites WR2, WR3, and WR4 are 33.4 +/- 1.9 (x10^{-15}), 27.5 +/- 1.5 (x10^{-15}), and 30.4 +/- 1.5 (x10^{-15}), respectively (Table 3, Fig. 8). The remaining river samples have $^{36}Cl/Cl$ ranging from 39.9 +/- 1.9 (x10^{-15}) to 94.8 +/- 3.5 (x10^{-15}; Table 3, Fig. 8). Two additional river sites have $^{36}Cl/Cl$ that fall outside the range for monthly precipitation. Site WR14 at Merom, IN has a low $^{36}Cl/Cl$, 39.9 +/- 1.9 (x10^{-15}), that is

Table 1
Field chemistry data for the Wabash River Watershed. 'ORUP' was collected in the Ohio River upstream of the confluence of the Wabash River and 'ORDN' was collected downstream of the confluence. Elevation of the sampling sites are listed in meters above sea level (masl). The field data from the headwaters reach are shown in the red shaded cells.

Sample ID	Sample Location	UTM 16 T mE	UTM 16 T mN	Elev. (masl)	Temp. (°C)	pH	SpC (μS cm^{-1})	TDS (ppm)	DO (%)	DO (mg L^{-1})
WR1	Historic Anthony Wayne Parkway Roadside Park, Fort Recovery, OH	691,220	4,469,326	309	9.1	7.94	676	439	65.7	7.6
WR2	Fort Site Park, Fort Recovery, OH	688,103	4,476,187	278	9.9	8.14	868	564	84.0	9.5
WR3	Ceylon Bridge, Ceylon, IN	674,238	4,498,051	250	10.3	7.99	829	539	59.1	6.5
WR4	Historic Forks of the Wabash, Huntington, IN	623,519	4,526,130	215	12.7	7.99	1051	683	82.5	8.6
WR5	West City Park, Peru, IN	577,024	4,510,339	194	11.9	8.21	493	320	85.3	8.9
WR6	France Park, Logansport, IN	546,150	4,511,076	172	14.8	8.14	637	414	67.8	6.9
WR7	Davis Ferry Park, Lafayette, IN	511,124	4,480,531	157	14.9	8.50	587	382	87.8	8.8
WR8	Granville Park, West Lafayette, IN	496,907	4,473,555	156	15.4	8.53	581	378	96.5	9.6
WR9	Ouabache Park, Attica, IN	478,264	4,460,423	153	15.2	8.60	585	380	97.7	9.7
WR10	Five Crossings Park, Covington, IN	465,592	4,442,991	149	15.5	8.60	580	377	100	10
WR11	Reeder Park, Montezuma, IN	468,034	4,404,105	146	16.9	8.62	604	393	103	9.9
WR12	Fairbanks Park, Terre Haute, IN	463,866	4,367,517	135	11.7	7.99	1246	810	90.2	9.7
WR13	Darwin Ferry, Darwin, IL	447,333	4,348,360	136	11.9	8.05	1255	816	79.0	8.6
WR14	Bluff Park, Merom, IN	450,546	4,323,289	131	11.4	8.07	1255	816	67.7	7.0
WR15	Kimmel Park, Vincennes, IN	454,822	4,283,104	125	11.4	8.05	1233	801	81.9	8.9
WR16	Mt. Carmel Wildlife Refuge, Mt. Carmel, IL	432,729	4,248,054	119	11.2	7.71	1223	795	50.8	5.6
WR17	Boat Ramp, New Harmony, IN	417,453	4,240,638	113	11.5	7.73	1061	690	63.2	7.0
WR18	New Haven, IL	404,614	4,187,753	106	11.7	7.51	702	456	55.4	6.0
ORUP	Ohio River, River Bend Park, Mt. Vernon, IN	421,472	4,198,255	108	13.5	7.78	979	636	84.7	8.6
ORDN	Ohio River, Boat Ramp, Old Shawneetown, IL	406,075	4,172,741	102	12.4	7.74	922	599	75.0	8.0

similar to the headwaters reach; while site WR18 at New Haven, IN has a higher $^{36}Cl/Cl$ of 94.8 +/- 3.5 (x10^{-15}; Table 3).

4.3. Spatial trends in $^{87}Sr/^{86}Sr$

At site WR1, the $^{87}Sr/^{86}Sr$ is 0.709080 (Table 4) falling between that of the glacial sediment (0.709783, purple triangle in Fig. 9) and the Silurian Wabash Formation (0.708778; orange square in Fig. 9). The $^{87}Sr/^{86}Sr$ ratios decrease downstream of WR1 and reach a minimum at WR3; the ratios then gradually increase downstream of WR4 (Fig. 9). Sites WR2, WR3, and WR3 of the headwaters reach have $^{87}Sr/^{86}Sr$ of 0.708904, 0.708530, and 0.708609, respectively. These ratios are similar to the dolomitic limestone samples of the early Silurian Wabash Formation and late Silurian Brassfield Formation (0.708292, green square in Fig. 9). The $^{87}Sr/^{86}Sr$ ratios of these Silurian rock-leachate samples closely match the $^{87}Sr/^{86}Sr$ seawater curve for the Silurian era reported in Burke et al. (1982) and McNutt et al. (1987). The $^{87}Sr/^{86}Sr$ of the headwater sites are not similar to either the Ordovician dolostone (0.710589, black diamond in Fig. 9) or Trenton brines (0.70901 to 0.71034, grey shaded box in Fig. 9) reported in McNutt et al. (1987). The remaining river samples have $^{87}Sr/^{86}Sr$ similar to glacial sediment (Fig. 9, Table 4). Some samples in the LWR have $^{87}Sr/^{86}Sr$ that fall within the grey box for Trenton brines; however, these sample sites are located far from the Trenton Gas Field and are, therefore, not associated with oilfield brines.

4.4. Spatial trends in $\delta^{18}O$ and $\delta^{2}H$ of water

The $\delta^{18}O$ and $\delta^{2}H$ compositions of all river sites are plotted in Fig. 10 relative to the global meteoric water line (GMWL, solid line in Fig. 10a; Craig, 1961) and the non-weighted local meteoric water line (LMWL, dashed line in Fig. 10) for West Lafayette, IN (Welp-Smith et al., 2020). Time series datasets of stable isotopes measured in precipitation are not available for the headwaters reach. The samples from the headwaters reach are isotopically distinct from the remainder of the river samples. In fact, WR1, WR2, WR3, and WR4 all cluster together and have $\delta^{18}O$ values less than −7.65‰ and $\delta^{2}H$ values less than −45.2‰ (Fig. 10a). Site WR3 has the lowest (most negative) stable isotopic composition of the three sites in the headwaters reach ($\delta^{18}O$ = -8.15‰ and $\delta^{2}H$ = -53.0‰; Table 5). Two of the remaining downstream river sites are isotopically heavy relative to the other river samples. Site WR5, located immediately downstream of the headwaters reach, has a $\delta^{18}O$ of −4.79‰ and $\delta^{2}H$ of –32.8‰), while WR16, located in the Lower Wabash, has a $\delta^{18}O$ of −5.45‰ and $\delta^{2}H$ of −27.9‰ (Fig. 10a). The remaining river samples have isotopic compositions falling within a relatively narrow range (-7.05 < $\delta^{18}O$ < -5.82‰ and −44.9 < $\delta^{2}H$ < -35.6‰; Fig. 10a and Table 5). Seasonal, non-weighted precipitation endmembers from Welp-Smith et al. (2020) are plotted in Fig. 10b as average values +/- 1 standard deviation (Table 6). Despite considerable storm-to-storm (interstorm) variability in these seasonal precipitation endmembers, the samples from the headwaters reach (open red circles) plot closer to the average spring endmember as compared to the other river sites (open blue circles) which plot within the bounds of summer precipitation (Fig. 10b).

5. Discussion

5.1. Sources of salinity inferred from geochemistry data

5.1.1. Sources of elevated chloride, sodium, and potassium

Baseflow Cl^- concentrations in the three headwater sites range from 56.4 to 131 mg L^{-1} and are 1.9 to 4.3 times higher than measured elsewhere in the Wabash River. For regional context, these Cl^- concentrations are higher than the two samples collected in the much larger Ohio River above (37 mg L^{-1}; ORUP in Table 2) and below (29.2 mg L^{-1}; ORDN in Table 2) the confluence with the Wabash River. For a broader context, these Cl^- concentrations are higher than those reported for the Middle Rio Grande and portions of the Lower Rio Grande in New Mexico (Cl^- less than 75 mg L^{-1}) where deep sedimentary brines are thought to discharge to the Rio Grande (Hogan et al., 2007). The Cl^-/Br^- mass ratios of the headwaters reach (758 to 1139) are also surprisingly high compared to the remainder of the watershed. In comparison, clean shallow groundwater (unaffected by pollution) collected in the middle reaches of the Wabash River watershed have Cl^-/Br^- ranging from 52 to 92.

One potential explanation for the elevated Cl^-/Br^- ratios of the headwaters reach is septic effluent and/or the discharge of brines from home water softener systems in septic effluent. Davis et al. (1998) report

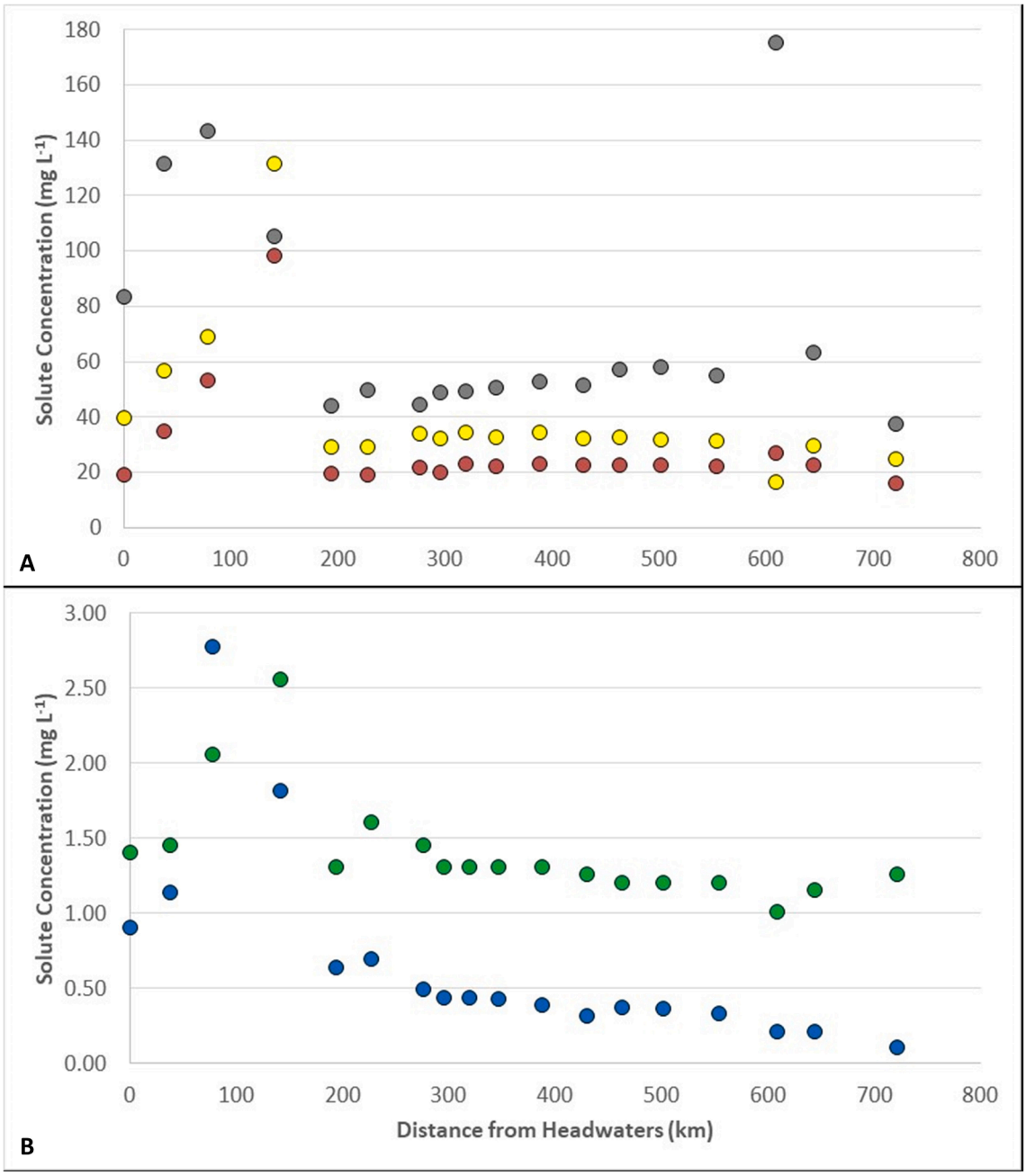

Fig. 7. Solute concentrations (mg L^{-1}) versus distance from headwaters measured along the main channel of the Wabash River. A) Grey circles represent sulfate, yellow circles represent chloride, and red circles represent sodium. B) Blue circles represent strontium and green circles represent fluoride × 5. (For interpretation of the references to colour in this figure legend, the reader is referred to the web version of this article.)

that the Cl^-/Br^- of domestic sewage commonly ranges between 300 and 600. For comparison, Vengosh and Pankratov (1998) reported Cl^-/Br^- for domestic sewage in Israel ranging from 410 to 873. For a regional comparison, Panno et al. (2006) reported Cl^-/Br^- of 403 to 533 for septic effluent in northeastern Illinois, although private septic systems had ratios ranging from 65 to 5404 where the highest ratios were due to the discharge of brine solution from water softener systems installed in the homes (see Harrison, 2006 for a description on how water softeners work). A simple divalent/monovalent cation mass ratio (D/M ratio) can be created from $(Ca^{2+} + Mg^{2+})/(Na^+ + K^+)$ to differentiate untreated (hard) from treated (softened) water. For example, water samples were analyzed before and after a water softener was installed in the home of the author for reference (Table 7). The untreated water has a D/M ratio of 4.1 and the treated water has a D/M ratio of 0.67 illustrating the substantial reduction (adsorption) of divalent ions in the water after treatment. Water samples from WR2, WR3, and WR4 have D/M ratios of 2.77, 1.73, and 1.07, respectively; whereas the average D/M ratio of the remaining river sites is 3.53 +/- 0.75 and range from 1.72 (near the confluence with the Ohio River at WR18) to 4.69 (WR1). Ultimately, it's unlikely that the D/M ratios in the headwaters reach result from brine effluent from home water softener systems due to the sparse population of the region. This type of effluent may have localized impacts, but we suspect that the brine becomes diluted in the larger aquifer or once it reaches a river. It's unlikely that septic effluent alone is responsible for the high Cl^-/Br^- ratios observed in the headwaters reach since it is located in open farmland and is not heavily populated except for the town of Huntington, IN.

Schnoebelen and Krothe (1999) state that non-reef portions of the

Table 2
Aqueous geochemical data for the Wabash River watershed. All solute concentrations are listed in mg L^{-1}. The analytical uncertainty relative to standards is shown beneath the ion in '+/- x' and the detection limits are shown in brackets. 'C.B.' is charge balance. The field data from the headwaters reach are shown in the red shaded cells.

Site ID	Ca^{2+} +/- 5 [0.05]	Mg^{2+} +/- 4 [0.05]	K^+ +/- 7 [0.05]	Na^+ +/- 5 [0.05]	Sr^{2+} +/- 4 [0.005]	Br^- +/- 6 [0.01]	Cl^- +/- 5 [0.1]	F^- +/- 6 [0.1]	NO_3^- +/- 4 [0.1]	SO_4^{2-} +/- 6 [1.0]	HCO_3^- +/- 4 [5.0]	Si +/- 9 [0.05]	C.B. (%)
WR1	90.4	22.4	5.34	18.7	0.899	0.040	39.4	0.28	25.8	82.9	255	10.4	−1.2
WR2	97.5	30.9	11.8	34.6	1.13	0.052	56.4	0.29	64.4	131	218	8.79	0.24
WR3	75.4	32.1	9.32	52.8	2.77	0.091	68.7	0.41	8.91	143	247	5.39	−1.3
WR4	82.6	29.5	7.03	97.8	1.81	0.115	131	0.51	30.10	105	286	8.42	−0.90
WR5	59.8	19.9	4.89	19.3	0.633	0.059	29.0	0.26	4.51	43.7	237	2.19	−1.0
WR6	81.8	25.1	4.35	18.9	0.692	0.126	28.9	0.32	8.55	49.2	320	4.27	−1.3
WR7	74.9	24.6	4.72	21.4	0.488	0.091	33.6	0.29	4.09	43.9	291	2.13	0.68
WR8	70.7	23.0	4.13	19.5	0.432	0.074	31.9	0.26	4.44	48.4	294	2.91	−3.3
WR9	71.0	22.9	4.16	22.7	0.432	0.025	34.2	0.26	5.31	49.1	278	2.86	−0.98
WR10	72.5	23.5	4.07	21.6	0.423	0.061	32.4	0.26	5.31	50.2	283	3.26	−0.84
WR11	72.4	24.4	3.89	22.7	0.383	0.067	33.9	0.26	6.01	52.6	291	3.43	−1.7
WR12	68.7	25.4	3.55	22.2	0.308	0.064	31.9	0.25	7.80	51.2	283	3.03	−1.4
WR13	72.2	25.0	3.71	22.3	0.362	0.069	32.1	0.24	6.01	56.8	289	3.15	−1.5
WR14	71.9	24.4	3.75	22.1	0.357	0.017	31.3	0.24	6.04	57.8	283	3.59	−1.5
WR15	71.1	24.3	4.20	21.9	0.322	0.019	31.1	0.24	6.19	54.7	278	4.50	−0.61
WR16	59.5	24.4	5.09	26.6	0.208	0.039	16.3	0.20	4.87	175	130	6.89	−0.59
WR17	54.0	18.7	5.14	22.4	0.204	0.064	29.1	0.23	5.89	62.9	203	5.62	−2.2
WR18	31.7	10.5	8.97	15.6	0.103	0.038	24.6	0.25	5.68	37.3	114	6.89	−1.8
ORUP	44.7	13.8	3.72	29.1	0.281	0.083	37.0	0.21	4.22	82.7	125	0.84	−1.8
ORDN	45.5	14.2	5.18	21.8	0.212	0.041	29.2	0.22	4.89	59.0	153	3.63	−1.6

Table 3
$^{36}Cl/Cl$ and Cl^- dataset for the sampling sites in the Wabash River watershed and monthly-integrated precipitation samples. $^{36}Cl/Cl_{unc}$ is the analytical uncertainty for the measured $^{36}Cl/Cl$. All Cl^-/Br^-, K^+/Cl^-, and $(K^+ + Na^+)/Cl^-$ ratios are calculated as mass ratios (mg L^{-1}/mg L^{-1}).

Site ID	$^{36}Cl/Cl$ (x 10^{-15})	$^{36}Cl/Cl_{unc}$ (x 10^{-15})	Cl^-/Br^-	K^+/Cl^-	$(Na^+ + K^+)/Cl^-$
WR1	50.0	2.6	985	0.14	0.61
WR2	33.4	1.9	1085	0.21	0.82
WR3	27.5	1.5	755	0.14	0.90
WR4	30.4	1.5	1139	0.05	0.80
WR5	42.3	2.4	492	0.17	0.83
WR6	59.6	2.7	229	0.15	0.80
WR7	52.3	2.2	369	0.14	0.78
WR8	56.9	2.9	431	0.13	0.74
WR9	54.6	2.5	1368	0.12	0.79
WR10	51.9	2.5	531	0.13	0.79
WR11	52.3	3.3	506	0.11	0.78
WR12	45.5	2.5	498	0.11	0.81
WR13	55.5	2.6	465	0.12	0.81
WR14	39.9	1.9	1841	0.12	0.83
WR15	54.2	2.5	1637	0.14	0.84
WR16	77.3	3.2	418	0.31	1.94
WR17	49.9	2.5	455	0.18	0.95
WR18	94.8	3.5	647	0.36	1.00
ORUP	36.1	2.3	444	0.10	0.89
ORDN	49.6	2.1	714	0.18	0.92
April 2015	69.1	3.6	–	–	–
May 2015	68.3	3.5	–	–	–
June 2015	43.2	2.8	–	–	–
July 2015	46.3	2.3	–	–	–
Aug. 2015	79.8	3.8	–	–	–
Sept. 2015	43.7	2.4	–	–	–
Oct. 2015	55.4	3.1	–	–	–

Silurian-Devonian carbonate aquifer in northwestern Indiana contain layers of interbedded montmorillonite and that these clay layers have a high cation exchange capacity. They attribute sodium-rich groundwater found in the non-reef carbonate aquifer to cation exchange processes occurring in the clay layers. It's plausible that elevated Na^+, and possibly at least some of the K^+, may originate from a similar process in the Silurian-Devonian carbonate aquifer in northeastern Indiana. Eberts and George (2000) state that sodium-rich groundwater found in the study area is due to cation exchange processes occurring in Devonian shales and subsequent mixing of waters in the carbonate aquifer. Unfortunately, we do not have bedrock cores to test this explanation.

Road salt (halite) is used as a deicer throughout the UWR during the winter. In addition, oilfield brines have historically been used as road deicers in the winter and as dust-control agents on country roads in the summer in northwestern Ohio (Kell et al., 2004), but brines are not used as deicers today. The dissolution of halite increases both the Cl^- concentration and Cl^-/Br^- in water but dilutes the $^{36}Cl/Cl$ in water. Davis et al. (1998) reported that halite dissolution results in Cl^-/Br^- mass ratios ranging from 1000 to 10,000. Samples of halite obtained for this study were dissolved in deionized water and found to have Cl^-/Br^- of 6060 and 6091 consistent with the range reported by Davis et al. (1998). Given the geologic age of these halite deposits, they should be ^{36}Cl-dead ($^{36}Cl/Cl = 0$). These halite samples had $^{36}Cl/Cl$ of 2.39 +/- 0.51 (x 10^{-15}) and 2.43 +/- 0.49 (x 10^{-15}). Bedded halite, if present in Silurian bedrock in northeastern IN, would be expected to have similar Cl^-/Br^- and $^{36}Cl/Cl$ approximately equal to 0. However, bedded halite deposits have not been mapped in the Silurian units of northeastern IN. Therefore, a geologic explanation in the Silurian bedrock for the observed salinity is tenuous at best. Alternatively, the elevated Cl^- and Cl^-/Br^- could potentially come from oilfield brines in the underlying Ordovician bedrock. However, the $^{87}Sr/^{86}Sr$ data argue against Trenton oilfield brines as a source for the observed salinity since the river samples do not fall within the range shown in the grey shaded box (data from McNutt et al., 1987) in Fig. 9. Thus, Trenton oilfield brines are not likely the source of the observed salinity.

Fertilizers, such as muriate of potash (KCl), can also contribute excess Cl^- to the headwaters reach via agricultural runoff or subsurface tile-drains. Samples of potash were not analyzed during this study; however, Panno et al. (2006) report a Cl^-/Br^- of 510 for potash. In that same study, Cl^-/Br^- ranged from 108 to 1974 for tile-drainage from agricultural fields in northeastern Illinois. In this study, the mass ratio of K^+/Cl^- ranges from 0.05 to 0.21 in the headwaters reach, whereas the $(Na^+ + K^+)/Cl^-$ ranges from 0.80 to 0.90. This would suggest that the Cl^- is sourced primarily from NaCl rather than potash fertilizers (Table 3). However, the $(Na^+ + K^+)/Cl^-$ ratio can be misleading since potassium and sodium do not behave conservatively or similarly in agricultural landscapes. Potassium is an essential nutrient for all plants (Hawkesford et al., 2012) while sodium is not essential for most crop plants (Maathuis, 2014). Although data for Na^+ and Cl^- concentrations

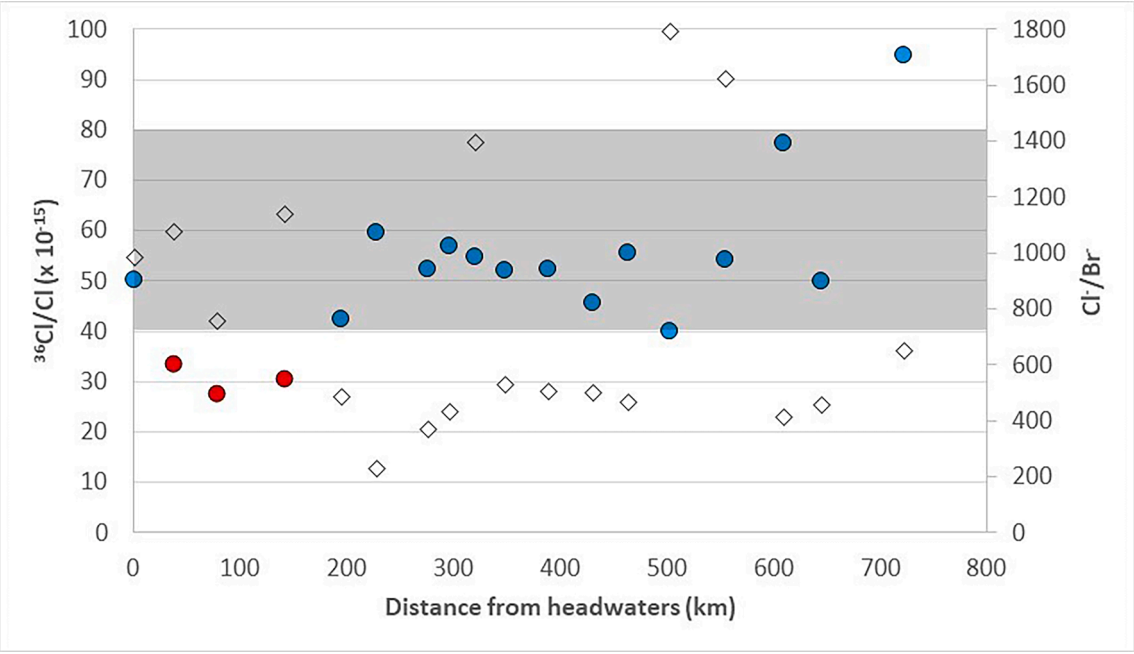

Fig. 8. $^{36}Cl/Cl$ and Cl^-/Br^- versus distance from headwaters measured along the main channel of the Wabash River. $^{36}Cl/Cl$ of river samples are shown by circles; the red circles represent the headwaters reach samples and the blue circles represent the remaining river samples. Cl^-/Br^- data are shown by open diamonds. The grey shaded area represents the range of $^{36}Cl/Cl$ for monthly-integrated precipitation collected during this study. (For interpretation of the references to colour in this figure legend, the reader is referred to the web version of this article.)

Table 4
$^{87}Sr/^{86}Sr$ dataset for the Wabash River watershed. [1]The $^{87}Sr/^{86}Sr$ data for precipitation was reported in *Sherman et al.* [2015]. [2]The glacial sediment end-member is leachate from a mixed gravelly till and clay-rich till sample. [3]The 'SBF' refers to a dolomitic limestone sample from the Silurian Brassfield Formation (whole rock $^{87}Sr/^{86}Sr$ analyses), the 'SWF' refers to a dolomitic limestone sample from the Silurian Wabash Formation (whole rock $^{87}Sr/^{86}Sr$ analyses), and the 'OPF' refers to a dolostone sample from the Ordovician Platteville Formation (whole rock $^{87}Sr/^{86}Sr$ analyses).

Site ID	$1/Sr^{2+}$ (L mg^{-1})	$^{87}Sr/^{86}Sr$	$^{87}Sr/^{86}Sr$ Uncertainty
WR1	1.11	0.709080	0.000029
WR2	0.885	0.708904	0.000025
WR3	0.361	0.708530	0.000024
WR4	0.552	0.708609	0.000024
WR5	1.58	0.708812	0.000026
WR6	1.45	0.708703	0.000024
WR7	2.05	0.708875	0.000029
WR8	2.31	0.708891	0.000036
WR9	2.31	0.708886	0.000030
WR10	2.36	0.708912	0.000021
WR11	2.61	0.708984	0.000035
WR12	3.25	0.709124	0.000050
WR13	2.76	0.709021	0.000027
WR14	2.80	0.709022	0.000030
WR15	3.11	0.709066	0.000022
WR16	4.81	0.710702	0.000045
WR17	4.90	0.709350	0.000028
WR18	9.71	0.710007	0.000036
ORUP	3.56	0.710925	0.000031
ORDN	4.72	0.710184	0.000045
Precipitation Dexter, MI[1]	–	0.709966	0.00036
Precipitation Detroit, MI[1]	–	0.708785	0.00039
Glacial Sediment (Leachate)[2]	–	0.709783	0.000034
SBF (Whole Rock)[3]	–	0.708292	0.000047
SWF (Whole Rock)[3]	–	0.708778	0.000034
OPF (Whole Rock)[3]	–	0.710586	0.000015

of soybean and corn grain are sparse, what data is available shows that K^+ concentration in grain exceeds that of Na^+ and Cl^- by approximately 1 to 2 orders of magnitude (Pietz et al., 1978; Parker et al., 1983, 1985; Yang and Blanchar, 1993). Crop plants take up K^+ and a proportion of this K^+ is removed in the grain and subsequently leaves the field. Ultimately, the $(Na^+ + K^+)/Cl^-$ ratio does not account for the uptake/removal ratio of K^+ by plants. In studies investigating sources of Cl^- in watersheds, it's common to see either 1) plots of K^+ vs Cl^- compared to plots of Na^+ vs Cl^-, 2) Na^+/Cl^- ratios compared to K^+/Cl^- ratios (shown here), or 3) attempts to close Cl^- mass balances at the watershed scale. If the effects of uptake/removal ratios of K^+ per crop are not considered, then the impact of KCl applications on the Cl^- load at the watershed scale will be underestimated.

Recommended rates of potash application to crops in Indiana are made based on soil test K^+ (an estimate of plant available K^+) and are outlined in Culman et al. (2020). Applications are usually made uniformly to the soil surface in the months of November through April, annually for one crop season or biennially for two crop seasons. Typically, the fertilizer will either be left on the soil surface or incorporated into the upper 15 cm of the soil. Briefly, the objective of fertilization is to maintain an optimal level of soil test K^+ (100 to 170 mg kg^{-1} soil varying by soil cation exchange capacity) and then replace crop removal from the field, plus 20 lb K_2O acre (~20 kg K ha^{-1}). Corn and soybean K^+ removal from the field in the grain are estimated at 0.20 and 1.15 lb K_2O $bushel^{-1}$, respectively, equivalent to approximately 3.5 and approximately 18 kg K Mg^{-1} grain dry matter. Since the recommendations are geared to replace crop K^+ removal, only approximately 20 kg K^+ ha^{-1} of the K^+ applied is expected to remain in the field as K^+ (20–30% of that added) and most would be retained by the negative charge of the soil. This would tend to drive the K^+/Cl^- of agricultural runoff lower than expected based on fertilizer application rates. In contrast, only 2 to 10% of the Cl^- applied would be removed from the field in the grain and that left in the soil (90–98% of that added) would be repelled by the soil's negative charge, making it much more likely to move with water.

The headwaters reach flows through farmland in Adams, Wells, and Huntington counties in Indiana where the primary crops are soybeans

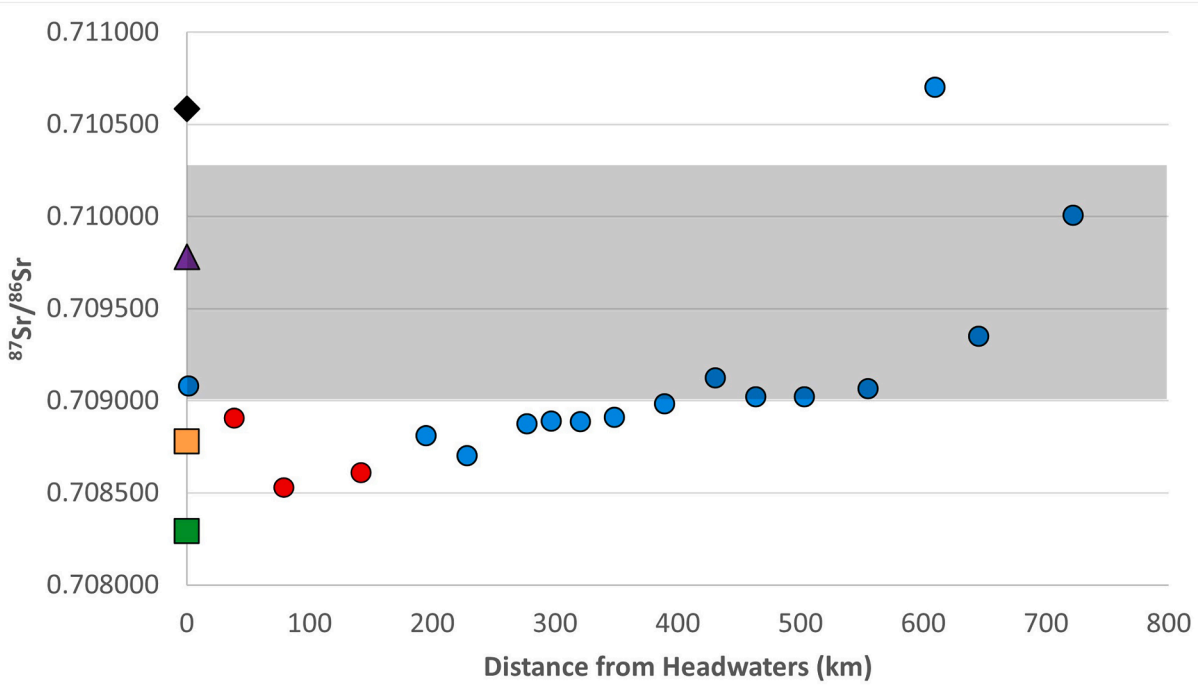

Fig. 9. $^{87}Sr/^{86}Sr$ in river samples versus distance from headwaters measured along the main channel of the Wabash River. Red circles represent the samples collected in the headwaters reach, while the blue circles represent the remaining river samples. The purple triangle represents the unconsolidated glacial sediment leachate, orange square represents the Silurian Wabash Formation (SWF), green square represents the Silurian Brassfield Formation (SBF), and the black diamond represents the Ordovician Platteville Formation (OPF). The shaded grey area represents the range of $^{87}Sr/^{86}Sr$ for Trenton brines (0.70901 to 0.71034) reported in McNutt et al. (1987). (For interpretation of the references to colour in this figure legend, the reader is referred to the web version of this article.)

and corn. In 2015, Adams County had 100,760 acres of soybeans and 67,962 acres of corn, Wells County had 116,635 acres of soybeans and 85,283 acres of corn, and Huntington County had 101,297 acres of soybeans and 61,315 acres of corn. In this region, approximately 150 lb KCl/acre (168 kg KCl/ha) would be recommended annually for soybean crops and approximately 75 lb KCl/acre (84 kg KCl/ha) for corn crops. Combined, this equates to approximately 34,094 U.S. tons (30,929 metric tons) of KCl that would be applied annually in these three counties alone. The vast majority of the potash used in this region, and in the Midwest, is mined from Devonian evaporite deposits in Saskatchewan (Fuzesy, 1982) and is supplemented with potash mined from Late Permian deposits in New Mexico (Austin, 1980). Given the geologic ages of these deposits, we can assume that the Cl^- present in the potash mined from these deposits is also ^{36}Cl dead. Thus, based on these data, potash is a plausible explanation for the high Cl^-, high Cl^-/Br^-, and $^{36}Cl/Cl$ dilution observed in the headwaters reach.

5.1.2. *Sources of elevated strontium, sulfate, fluoride, and nitrate*

The unique geochemical composition of the three headwater sites is apparent when the data are plotted in a piper diagram (Fig. 11). Despite their location in the headwaters of the watershed, their geochemical composition more closely matches that of river sites in the LWR. The three headwater sites are calcium-sulfate type waters while the remaining river samples are calcium-bicarbonate type waters, except for WR16 (Fig. 11). Site WR16 likely has elevated SO_4^{2-} from coal-ash residuals and is an anomalous sample (discussed below). The Sr^{2+} and SO_4^{2-} concentrations measured in the headwaters reach are quite high relative to the remaining river samples. In general, Sr^{2+} concentrations tend to be very low in natural waters, often less than 0.10 mg L^{-1} (Hem, 1985). Foley et al. (1972) reported elevated Sr^{2+} and SO_4^{2-} in the bedrock aquifer of Allen County, IN located immediately north of the headwaters reach. However, Sr^{2+} concentrations in the unconsolidated glacial aquifers of Allen County tended to be very low in comparison. In that study, they attributed the anomalous concentrations of Sr^{2+} and SO_4^{2-} in the bedrock aquifer to the dissolution of celestite ($SrSO_4$) and/or strontianite ($SrCO_3$) present in the carbonate bedrock. The Findlay Arch mineral belt contains abundant celestite (Carlson, 1987; 1994), however celestite has a relatively low solubility compared to gypsum (Dove and Czank, 1995) which may limit its contribution to the Sr^{2+} and SO_4^{2-} load to groundwater and surface water. Schnoebelen and Krothe (1999) analyzed groundwater from bedrock in Silurian-Devonian bedrock in northwestern Indiana. They did not observe elevated Sr^{2+} (0.41 to 0.63 mg L^{-1}) in the non-reef Silurian-Devonian aquifer, but they did report elevated SO_4^{2-} (150 to 170 mg L^{-1}). Feulner and Hubble (1960) and *OH EPA* (2012) both report high Sr^{2+} concentrations in groundwater from Silurian carbonate aquifers in western Ohio (southeast of Fort Recovery, OH) due to the presence of celestite and strontianite in the bedrock. Luczaj and Masarik (2015) also suggest that celestite (and possibly strontianite) are responsible for elevated Sr^{2+} concentrations in groundwater in eastern Wisconsin, however their groundwater samples were collected from older Cambrian-Ordovician sandstones.

Sacks and Tihansky (1996) analyzed concentrations of Sr^{2+} and SO_4^{2-} in samples of gypsum collected from the Upper Floridan Aquifer that were dissolved in deionized water. They report Sr^{2+}/SO_4^{2-} molar ratios of 1 for celestite and 0.003 in gypsum (explained by limited replacement of Ca^{2+} with Sr^{2+} in gypsum). We ground samples of carbonate rocks collected in the headwaters of the Wabash River from the Ordovician Platteville Formation, Silurian Wabash Formation, and Silurian Brassfield Formation and dissolved them in deionized water in a similar fashion. The leachates yielded Sr^{2+}/SO_4^{2-} molar ratios of 0.002, 0.004, and 0.037, respectively. In addition, Frisbee et al. (2019) collected water samples from three karst springs emerging from the Wabash Formation near Site WR6 in Logansport, IN. These three springs had Sr^{2+}/SO_4^{2-} molar ratios ranging from 0.005 to 0.008 consistent with the rock leachate from the Silurian Wabash Formation. In comparison, Sites WR2, WR3, and WR4 had Sr^{2+}/SO_4^{2-} molar ratios of 0.009, 0.021, and 0.019, respectively which are, again, similar to the

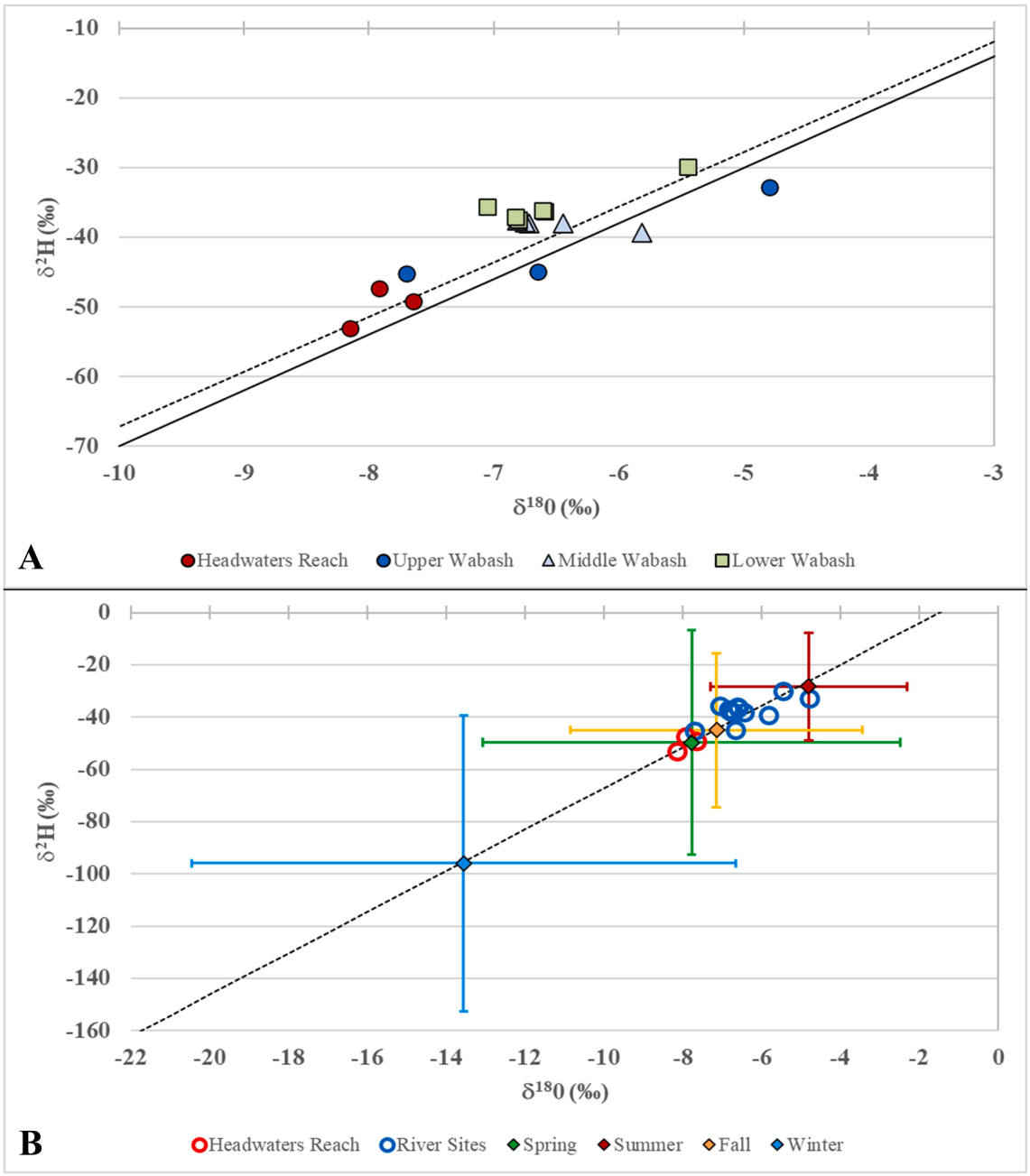

Fig. 10. A) Stable isotopic composition of river samples relative to the GMWL [solid line; Craig, 1961] and non-weighted LMWL [dashed line; Welp-Smith et al., 2020] given by: $\delta^2H = 7.97 \times \delta^{18}O + 11.7$; $r^2 = 0.99$, based on data collected from 2015 to 2019. B) River samples plotted against non-weighted average seasonal endmembers for West Lafayette, IN. River samples are open circles; red circles represent the headwaters reach and the blue circles represent the remaining river samples. Non-weighted average seasonal precipitation endmembers (+/- one standard deviation) are represented by diamonds. (For interpretation of the references to colour in this figure legend, the reader is referred to the web version of this article.)

Silurian rock leachates. The three headwater sites have the highest Sr^{2+}/SO_4^{2-} molar ratios in the entire watershed. Site WR1 has a Sr^{2+}/SO_4^{2-} molar ratio of 0.012 and the ratios decrease progressing downstream of WR4. Therefore, the dissolution of gypsum can potentially explain the higher concentrations of strontium and sulfate.

Only one sampling site in the LWR has a SO_4^{2-} concentration comparable to the headwater reach. That site, WR16, has a SO_4^{2-} concentration of 175 mg L^{-1} and is located immediately downstream of a coal-burning power plant near Mt. Carmel, IL. This site also has an elevated $^{87}Sr/^{86}Sr$ ratio (0.710702) that is consistent with the range of coal combustion residuals (CCR) from the Illinois Basin reported in Ruhl et al. (2014) and Harkness et al. (2016). High SO_4^{2-} concentrations were also reported in plumes from a coal-fired power plant in Portage, WI (Simsiman et al., 1987). A water sample collected concurrently in the White River upstream of its confluence with the Wabash River and upstream of the coal-burning power plant near Mt. Carmel, IL has a $^{87}Sr/^{86}Sr$ of 0.709359 and a SO_4^{2-} concentration of 74 mg L^{-1} for comparison. The elevated SO_4^{2-} and high $^{87}Sr/^{86}Sr$ at Site WR16 are consistent with coal-ash residuals.

The Findlay Arch mineral belt also contains abundant fluorite (Carlson, 1994). Fluorite has a low solubility and fluoride concentrations tend to be very low (< 1.0 mg L^{-1}) in natural waters having TDS less than 1000 mg L^{-1} (Hem, 1985). However, elevated F^- concentrations (ranging up to 4 mg L^{-1}) have been reported in wells installed in

Table 5
$\delta^{18}O$ and $\delta^{2}H$ dataset for river sites in the Wabash River watershed. The analytical uncertainty ($\delta^{18}O_{unc}$ and $\delta^{2}H_{unc}$) shown here is calculated as the average variability of the final six measurements. 'D-excess' is deuterium excess given by: $\delta^{2}H - (8 \times \delta^{18}O)$.

Site ID	$\delta^{18}O$ (‰)	$\delta^{18}O_{unc}$ (‰)	$\delta^{2}H$ (‰)	$\delta^{2}H_{unc}$ (‰)	D-excess
WR1	−7.70	0.14	−45.2	0.1	16.34
WR2	−7.92	0.18	−47.3	0.4	16.06
WR3	−8.15	0.10	−53.0	0.4	12.21
WR4	−7.65	0.10	−49.1	0.2	12.04
WR5	−4.79	0.04	−32.8	0.3	5.52
WR6	−6.65	0.05	−44.9	0.4	8.27
WR7	−6.79	0.04	−37.7	0.3	16.65
WR8	−6.72	0.10	−38.0	0.4	15.70
WR9	−6.44	0.09	−38.0	0.3	13.55
WR10	−6.75	0.09	−37.9	0.2	16.14
WR11	−6.81	0.06	−37.6	0.3	16.95
WR12	−5.82	0.07	−39.3	0.4	7.25
WR13	−6.80	0.09	−37.5	0.3	16.96
WR14	−6.83	0.12	−37.1	0.4	17.49
WR15	−6.59	0.13	−36.3	0.4	16.48
WR16	−5.45	0.25	−29.9	0.8	13.66
WR17	−6.61	0.09	−36.2	0.3	16.70
WR18	−7.05	0.05	−35.6	0.2	20.86
ORUP	−7.37	0.05	−39.2	0.4	19.71
ORDN	−6.75	0.06	−35.7	0.1	18.32

Silurian and Devonian rocks in northwestern Ohio in close proximity to the headwater reach (OH EPA, 2012). The F^- concentrations for sites WR2, WR3, and WR4 were 0.29 mg L^{-1}, 0.41 mg L^{-1}, and 0.51 mg L^{-1}, respectively. All but one of the remaining river sites have F^- less than 0.29 mg L^{-1}. Schnoebelen and Krothe (1999) provide an alternative explanation for high F^- concentrations (2.4 to 3.1 mg L^{-1}) observed in the non-reef Silurian-Devonian aquifer in northwestern Indiana. They state that the high F^- can be explained by apatite instead of fluorite. In their study, the groundwater samples were undersaturated with respect to fluorite and positive with respect to apatite. In principle, PO_4^{3-} concentrations should increase as apatite is weathered. However, our samples were not field acidified and therefore nearly all the sites were non-detects with respect to PO_4^{3-}. In any case, there is a plausible geologic explanation for the relatively high F^- concentrations observed in the headwaters reach.

Reconciling the apparent disagreement on the source of the high Cl^-, high Cl^-/Br^-, and low $^{36}Cl/Cl$ and the source of the high Sr^{2+}, SO_4^{2-}, and F^- is difficult. However, NO_3^- provides additional insight. The NO_3^- concentrations in the headwaters reach are also high relative to the remaining river sites. Site WR1 has a NO_3^- concentration of 25.8 mg L^{-1} while Sites WR2, WR3, and WR4 have concentrations of 64.4, 8.91, and 30.1 mg L^{-1}, respectively. Site WR3 is again distinct from WR2 and WR4 in that it has the lowest NO_3^- concentration. The remaining downstream river sites have NO_3^- concentrations ranging from 4.09 to 8.55 mg L^{-1} with an average concentration of 5.76 +/- 1.23 mg L^{-1}. Elevated NO_3^- is an indicator of nutrient-rich runoff or legacy nutrients in groundwater. These data again seem at odds with the concentrations of Sr^{2+} and SO_4^{2-} which are not likely due to anthropogenic effects found in the study area. One plausible explanation for Sites WR2 and WR4 is that groundwater discharging to the river from the Silurian carbonate regional aquifer mixes with shallow groundwater that has been contaminated over time with Cl^- and NO_3^- from agricultural practices. This would preserve the high Cl^-, high Cl^-/Br^-, low $^{36}Cl/Cl$ and the high Sr^{2+}, SO_4^{2-}, Mg^{2+}, and F^-. However, Site WR3 does not conform to this conceptual model.

5.2. Sources of salinity inferred from Isotope data

River samples are plotted relative to the LMWL (dashed line), GMWL (solid line), and seasonal endmembers in Fig. 10b. The storm-to-storm (interstorm) variability in the seasonal precipitation endmembers is quite high (Fig. 10b; Welp-Smith et al., 2020). Winter and spring precipitation have the lightest minimum $\delta^{18}O$ values (−26.3 and –22.4‰, respectively), yet winter precipitation also has the largest interstorm variability of all seasonal endmembers. Summer precipitation has the heaviest (least negative) $\delta^{18}O$ and $\delta^{2}H$ composition and shows the least interstorm variability of the seasonal endmembers. The $\delta^{18}O$ and $\delta^{2}H$ compositions of WR1, WR2, WR3 and WR4 are lighter (more negative) than and distinct from the remaining downstream river samples (Fig. 10a). These four river samples plot closely with the average spring endmember (Fig. 10b). In comparison, the remaining river samples have $\delta^{18}O$ value more positive than −7.1‰ and plot between the average summer and average fall precipitation endmembers (Fig. 10b).

It's unlikely that much, if any, recharge occurs during the summer growing season (April through September) in northern Indiana because there is an increased water demand for crops and the summer months are typically the driest. In fact, Daniels et al. (1991) and Naylor et al. (2016) state that >65 percent of groundwater recharge in northern Indiana occurs from fall (October/November) to spring (March/April). Frisbee et al. (2017) found that a recharge temperature between 0 °C and approximately 4 °C provided the best fit to atmospheric CFC curves and yielded comparable CFC ages for the groundwater samples suggesting that little, if any, recharge occurs in the summer growing season. It's more likely that the $\delta^{18}O$ values of the downstream river samples reflect a large proportion of recent runoff. This inference is consistent with the $^{36}Cl/Cl$ data. Table 3 shows the $^{36}Cl/Cl$ of monthly precipitation from April to October of 2015. The minimum $^{36}Cl/Cl$ during this period was 43.2×10^{-15} and the maximum was 79.8×10^{-15} (this range is illustrated by the grey box in Fig. 8). The water samples were collected in the UWR in October 2015 when the monthly $^{36}Cl/Cl$ in precipitation was 55.4 $\times$ 10^{-15}. In comparison, the remaining downstream river samples have $^{36}Cl/Cl$ ranging from 39.9 +/- 1.9 (x 10^{-15}) to 94.8 +/- 3.5 (x 10^{-15}). This range is somewhat misleading since 11 of the 14

Table 7
Aqueous geochemical data for a home water softener system in West Lafayette, IN. All solute concentrations are listed in mg L^{-1}. Detection limits are shown in brackets.

Site ID	Ca^{2+} [0.05]	Mg^{2+} [0.05]	K^+ [0.05]	Na^+ [0.05]	$(Ca^{2+} + Mg^{2+})/(Na^+ + K^+)$
Untreated	90.0	27.5	3.7	25.2	4.1
Treated	14.8	4.12	15.5	12.9	0.67

Table 6
$\delta^{18}O$ and $\delta^{2}H$ dataset for precipitation collected near West Lafayette, IN (Welp-Smith et al., 2020).

	Spring (March – May)		Summer (June – August)		Fall (Sept. – Nov.)		Winter (Dec. – Feb.)	
	$\delta^{18}O$ (‰)	$\delta^{2}H$ (‰)	$\delta^{18}O$ (‰)	$\delta^{2}H$ (‰)	$\delta^{18}O$ (‰)	$\delta^{2}H$ (‰)	$\delta^{18}O$ (‰)	$\delta^{2}H$ (‰)
Average	−7.8	−50	−4.8	−28	−7.1	−45	−13.6	−96
Std. Dev.	5.3	43	2.5	21	3.7	30	6.9	57
Maximum	−0.7	5	−0.2	1	−0.7	12	0.5	13
Minimum	–22.4	−173	−11.5	−81	−16.3	−116	−26.3	−107

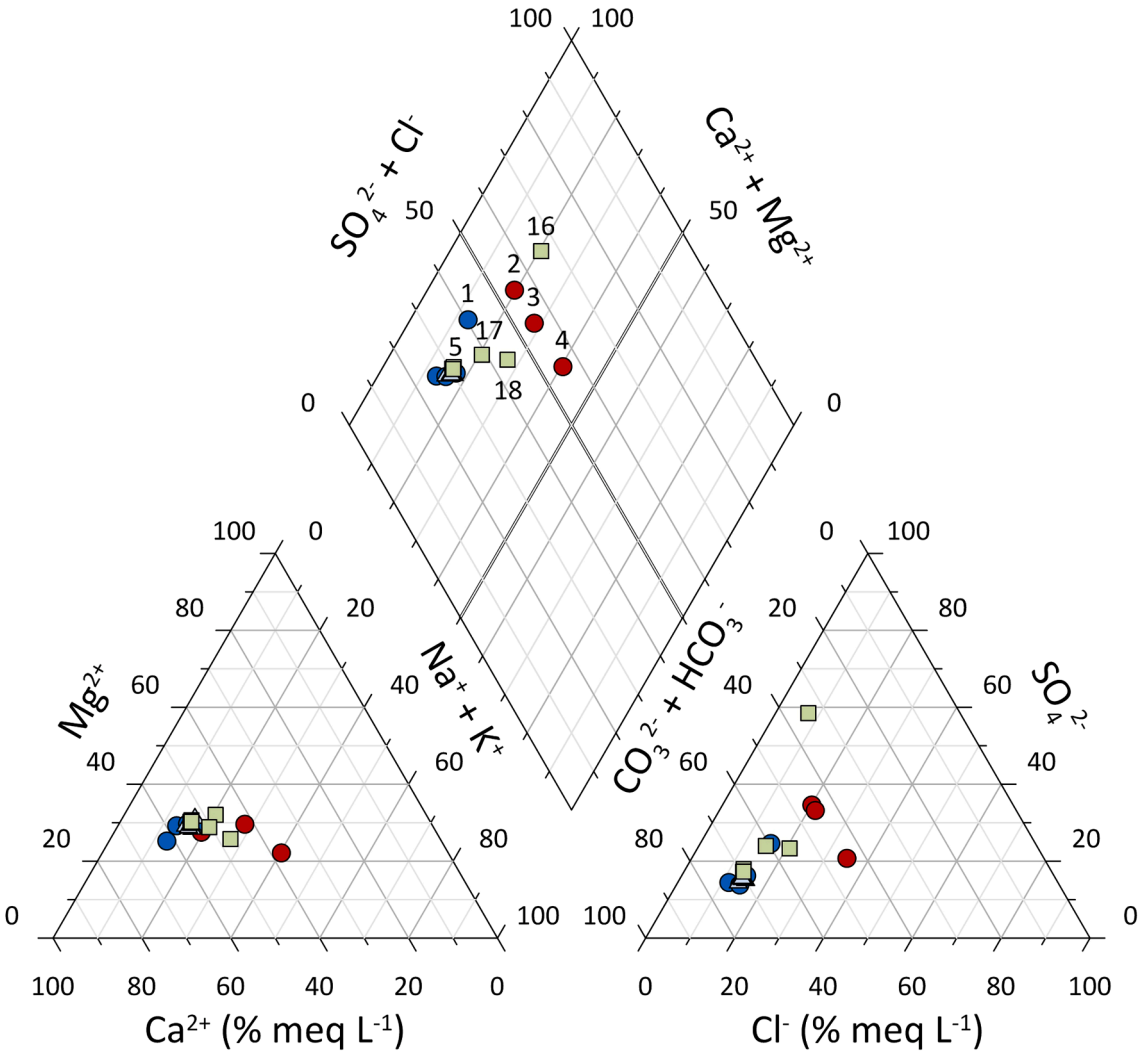

Fig. 11. Piper diagram of the river samples. Red circles represent the headwaters reach samples, blue circles represent the samples from the UWR, light blue triangles represent the samples from the MWR, and light green squares represent the samples from the LWR. Labels are not provided for all sampling sites to avoid clutter. Instead, only the sampling sites in the headwaters reach (1 = WR1, 2 = WR2, 3 = WR3, 4 = WR4, and 5 = WR5) and the sampling sites in the LWR (16 = WR16, 17 = WR17, and 18 = WR18) are provided for comparison. (For interpretation of the references to colour in this figure legend, the reader is referred to the web version of this article.)

downstream samples fall within the range of 42.3 × 10^{-15} to 59.6 × 10^{-15}, a range that is similar to that of monthly precipitation during this time (Table 3, Fig. 8). We infer that the downstream river samples contained a substantial component of recent runoff at the time of sampling.

Sites WR2, WR3, and WR4 have $^{36}Cl/Cl$ of 33.4 × 10^{-15}, 27.5 × 10^{-15}, and 30.4 × 10^{-15}, respectively. These ratios are even lower than the range for monthly precipitation collected in 2015 ranging from 43.2 × 10^{-15} to 79.8 × 10^{-15}. Davis et al. (2000) show $^{36}Cl/Cl$ data for five wells located northeast of Fort Wayne, IN. These wells were installed at depths of 6.1, 18.0, 24.4, 29.0, and 48.8 m deep. All but the deepest well was installed in unconsolidated glacial sediments; the 48.8 m well was screened into the underlying Devonian carbonate bedrock. They report $^{36}Cl/Cl$ of 12.6 +/- 2.9 (x 10^{-15}), 166 +/- 11 (x 10^{-15}), 153 +/- 8 (x 10^{-15}), 190 +/- 22 (x 10^{-15}), and 250 +/- 15 (x 10^{-15}), respectively and all but the 6.1 m deep well were tritium-dead. These groundwater samples had Cl^-/Br^- of 2720, 43.4, 47.8, 32.4, and 41.6, respectively. Davis et al. (2000) inferred that the low $^{36}Cl/Cl$, high Cl^-/Br^-, and high ^3H (16 TU) of the shallow well (6.1 m) resulted from an influx of Cl^--contaminated surface water. The higher $^{36}Cl/Cl$, lower Cl^-/Br^-, and ^3H-dead groundwaters of the remaining wells most likely resulted from the weathering of fluid inclusions in plutonic clasts in the unconsolidated glacial sediment. The $^{36}Cl/Cl$ of WR2, WR3, and WR4 are lower than the groundwater samples reported in Davis et al. (2000) and lower than 2015 precipitation samples reported here. We infer that these samples show the effects of ^{36}Cl dilution.

As mentioned earlier, it's unlikely that the old Cl^- originates from septic effluent and/or home water softener brine alone or bedded halite. In addition, the $^{87}Sr/^{86}Sr$ of WR2, WR3, and WR4 most closely match the $^{87}Sr/^{86}Sr$ of the Silurian Brassfield Formation (SBF) and Silurian Wabash Formation (SWF) and argue against a source in the Ordovician rocks or Ordovician oilfield brines. Ultimately, the two remaining sources that can potentially explain the low $^{36}Cl/Cl$ are old Cl^- from road salt or potash fertilizer. Given the application rates of KCl in the counties of the headwaters reach and the timing of the river sampling in late fall (prior to the winter use of deicers), KCl seems most plausible. We cannot discount the possibility of legacy Cl^- from road salt.

The unconsolidated thickness of the headwater reach may help reconcile these datasets. The unconsolidated sediment is relatively thin in the headwaters reach (Fig. 3) ranging from less than 1.0 to 154 m in the UWR (please note that Fig. 3 shows the minimum and maximum thickness in the window and not in the UWR alone). The unconsolidated

sediment is 28.2 m, 23.4 m, 43.7 m, and 17.0 m at Sites WR1, WR2, WR3, and WR4, respectively. This thin cover of glacial sediment would, in principle, increase the possibility that regional groundwater could be discharged to the Wabash River or allow it to mix with shallow groundwater. Hoyer and Hallberg (1991) state that bedrock aquifers in Iowa that are overlain by glacial sediment less than 30.5 m are more susceptible to contamination. If applied to Indiana, then this suggests that Sites WR1, WR2, and WR4 are likewise more susceptible.

Site WR3 does not conform to this conceptual model. This site is spatially located where the Ordovician Maquoketa Group Aquifer System has been mapped (Schmidt, 2009) and is spatially coincident with the buried channel of the ancient Teays River (Fidlar, 1943; Steeg, 1946; Bruns and Steen, 2003). At Ceylon, IN (north of Geneva, IN), the unconsolidated sediment is 43.7 m. Previous research indicates that the sidewalls of the buried Teays Valley in this area are steep and cut through Silurian Salamonie Dolomite into Ordovician carbonates and shales (Bruns and Steen, 2003). In northern IN, the Salamonie Dolomite overlies the Brassfield Formation thereby supporting the $^{87}Sr/^{86}Sr$ data. Site WR3 also has lower DO and SpC than the other sites in the headwaters reach, and much lower NO_3^- concentrations. If ture, then this suggests that the groundwater discharging from the Teays Valley sediment and carbonate bedrock aquifer may not be contaminated. If significant mixing were occurring between the shallow aquifers and deep, relatively clean groundwater from the regional carbonate aquifer, then we would expect WR3 to show similar effects as WR2 and WR4. In any case, a hydrogeologic connection is present between the headwaters of the Wabash River, the Silurian-Devonian carbonate aquifer, and the buried Teays Valley sediment at WR3. Without the aid of multiple isotopic tracers and geochemical data, this hydrogeologic connection would remain masked by the solute burden of the phreatic aquifer.

5.3. Baseflow separation models

A second goal of this study was to determine how much, if any, baseflow comes from the inferred sources of the salinity. To accomplish this task, we chose to use a $^{87}Sr/^{86}Sr$ mixing model. In the $^{87}Sr/^{86}Sr$ mixing model, we assumed that the strontium ratio for each river sample is equal to a mixture of shallow groundwater (phreatic aquifer in unconsolidated sediment) and regional groundwater (carbonate aquifer). We know the $^{87}Sr/^{86}Sr$ of glacial sediment in the region and the glacial sediment leachate should approximate the $^{87}Sr/^{86}Sr$ of the shallow aquifer, tile drains, and perhaps even surface runoff in the headwaters reach. Thus, if water infiltrates the glacial sediment, then it will slowly acquire the $^{87}Sr/^{86}Sr$ of the strontium-bearing minerals in the sediment. Therefore, we assume that the $^{87}Sr/^{86}Sr$ of the shallow aquifer is equivalent to the $^{87}Sr/^{86}Sr$ of leachate from glacial sediment (0.709783 +/- 0.000034). The regional groundwater endmember is assumed to be equivalent to the $^{87}Sr/^{86}Sr$ of the Silurian Brassfield Formation (0.708292 +/- 0.000047). The results of this two-endmember mixing model show that the fraction of regional groundwater in baseflow at WR2, WR3, and WR4 is 58, 84, and 79 percent, respectively. The highest contribution from regional groundwater is associated with WR3.

These estimates are conservative. First, as mentioned earlier, widespread flooding occurred throughout the UWR and MWR in 2015. While we have faith that baseflow conditions were present when the UWR was sampled (Fig. 4), it is difficult to determine what effect delayed subsurface runoff had on the isotopic and geochemical signature of baseflow in the headwaters. Repeat synoptic sampling campaigns should be completed to sample baseflow during a "normal" precipitation year and identify the contribution of groundwater from deep aquifers on baseflow in the remaining downstream sites. Second, while we have collected and analyzed a small subset of the rocks in the stratigraphic column, we may not have captured variability in $^{87}Sr/^{86}Sr$ present in different lithofacies. However, our data and interpretations of groundwater flow and geochemical processes largely conform to those of other studies in the same rock units. In any case, the $^{87}Sr/^{86}Sr$ data support a hydrogeologic connection between the headwaters of the Wabash River and the regional carbonate aquifer and show that there is a connection between the aquifer associated with the buried Teays Valley, regional carbonate aquifer, and river. Without the aid of multiple isotopic and geochemical tracers, the hydrogeologic connection between the river and the regional aquifer would have remained masked.

6. Conclusions

The main objectives of this research study were to address the following questions 1) what is the source of the anomalous solute concentrations and high salinity in the headwaters reach of the Wabash River, 2) what do the solute concentrations reveal about the sources of baseflow in the headwaters reach, and 3) how much, if any, groundwater from the regional aquifer is discharged to the headwaters reach? The most plausible explanation for the elevated Cl^- observed in the headwaters of the Wabash River is that it comes from an anthropogenic source. The timing of the sampling at the end of the growing season and prior to widespread application of road salt in winter suggests that KCl fertilizers are the likely source of the salinity. However, we cannot rule out the effects of legacy Cl^- from past road salt usage. In either case, an old source of Cl^- is responsible for the salinity and the observed ^{36}Cl dilution in the headwaters reach. Unfortunately, $^{36}Cl/Cl$ cannot, by itself, differentiate between the proportions of salinity coming from two ^{36}Cl-dead sources of salt.

With respect to the 2nd objective, baseflow generation processes in the headwaters of the Wabash River are spatially complex. The Cl^-, NO_3^-, Cl^-/Br^-, and $^{36}Cl/Cl$ data seem at odds with the F^-, Sr^{2+}, SO_4^{2-}, and $^{87}Sr/^{86}Sr$ data; the former point to anthropogenic effects while the latter point to geologic sources of solutes. The $^{87}Sr/^{86}Sr$ data support a hydrogeologic connection between the headwaters of the Wabash River and the regional carbonate aquifer. Sites WR2, WR3, and WR4 have $^{87}Sr/^{86}Sr$ ratios similar to Silurian carbonate rocks which host the Midwestern Basins and Arches Regional Aquifer System. In comparison, the $^{87}Sr/^{86}Sr$ steadily increase progressing downstream of the headwaters reach and gradually reach a $^{87}Sr/^{86}Sr$ similar to leachate from glacial sediment. In addition, the δ^2H and $\delta^{18}O$ compositions for the downstream sites are distinct from the headwaters reach and plot more closely to the average summer precipitation endmember suggesting again that these sites contain a large proportion of recent runoff. These data support our inference that the downstream river sites are comprised of a larger proportion of runoff or discharge of shallow groundwater from recent flooding. In comparison, Sites WR1, WR2, WR3, and WR4 have the lightest (most negative) δ^2H and $\delta^{18}O$ compositions and are similar to the average δ^2H and $\delta^{18}O$ composition of spring precipitation (cold season recharge). The retention of the light δ^2H and $\delta^{18}O$ composition in the headwaters reach is important. We infer that it points to groundwater discharged from the regional aquifer. It's plausible that the regional groundwater is a mixture of modern recharge and Pleistocene recharge based on the range for Pleistocene recharge presented in Eberts and George (2000). Our conceptual model for the headwaters reach is that the Cl^-, NO_3^-, Cl^-/Br^-, and $^{36}Cl/Cl$ are tracking anthropogenic sources of solutes discharged from shallow groundwater hosted in unconsolidated sediment, whereas the F^-, Sr^{2+}, SO_4^{2-}, and $^{87}Sr/^{86}Sr$ are tracking bedrock weathering processes in the underlying carbonate aquifer. At baseflow, mixing between shallow (Cl^- and NO_3^- rich) groundwater from the unconsolidated sediment and regional (Cl^- and NO_3^- poor) groundwater from the carbonate aquifer occurs in the river.

Site WR3 does not completely conform to this conceptual model. We infer that there is some communication between the river and groundwater associated with the buried Teays Valley at Site WR3. In fact, a greater proportion of deep groundwater is present in baseflow at Site WR3 based on the $^{87}Sr/^{86}Sr$ mixing model. Thus, with respect to the 3rd objective, we estimate that 58 to 84 percent of baseflow in the headwater reach comes from the regional groundwater discharged from the Silurian-Devonian carbonate aquifer (and buried Teays Valley sediment

at WR3). These estimates are conservative and additional synoptic sampling campaigns combined with sampling of groundwater wells are necessary to get a more complete understanding of seasonal variability in the sources of baseflow and salinity in the headwaters of the Wabash River. Without the aid of multiple isotopic and geochemical tracers, the hydrogeologic connection between the river and the regional aquifer would have remained masked. Forensic applications of multiple isotopes enhance the ability to "see" different reservoirs of water even in intensively-managed landscapes.

These findings have implications for the UWR and other agricultural watersheds. While the Intensively Managed Landscapes Critical Zone Observatory (IML-CZO) has substantially improved our understanding on how agricultural practices, such as tillage and subsurface drainage modifications, have impacted water, solute, and nutrient yields from agriculturally managed landscapes (Kumar et al., 2018; Wilson et al., 2018), these studies rarely quantify deep or regional groundwater processes. As a consequence, our understanding of their role in solute release, salinity, residence times, and agroecosystem integrity is incomplete. In addition, our understanding of the exchange of Cl^- and NO_3^- between phreatic aquifers and deeper aquifers remains incomplete. Further quantification of this groundwater component in agricultural watersheds will improve regional hydrological models, solute- and nutrient-loading models, and geochemical weathering models. It will also fill knowledge gaps in our understanding of baseflow generation processes in agricultural watersheds and improve salinity budgets in these same areas. On a local-scale, future investigations of the UWR should not ignore the discharge of groundwater from the regional carbonate aquifer or groundwater associated with the buried Teays Valley.

In the majority of agricultural watersheds, salinization can largely be explained by anthropogenic sources of salt. In the American Midwest, road salt and KCl fertilizers are usually identified as the primary sources of salinity. However, the role of KCl in salinization may be underestimated in studies where crop K^+ uptake/removal ratios are not considered. The uptake/removal of K^+ is very different than Na^+ for crops grown in the UWR; therefore, ratios of Na^+/Cl^-, K^+/Cl^-, or $(Na^+ + K^+)/Cl^-$ suggest that KCl has less of an impact on salinity. This seems at odds with the KCl application rates. While $^{36}Cl/Cl$ can be used to identify old sources of Cl^-, it cannot by itself discern between two sources of Cl^- that are both ^{36}Cl-dead. Future work should investigate coupling $^{36}Cl/Cl$ with other tracers to sort out the individual impacts of road salt versus KCl fertilizers. This problem is further exacerbated by our incomplete understanding of the roles of shallow and deep groundwater in baseflow generation in these settings. The salinity budget in agricultural watersheds is complicated by a continual exchange of water, salt, and nutrients between the land surface and shallow subsurface aquifers; however, there are few attempts to quantify the exchanges with deep aquifers. If exchanges of Cl^- between surface water, shallow aquifers, and deep aquifers are substantial, then future efforts to mitigate salinity increases in agricultural rivers will not be successful because there may be substantial storage of Cl^- in groundwater and it may be released slowly across long time scales.

CRediT authorship contribution statement

Marty D. Frisbee: Conceptualization, Methodology, Sample Collection, Writing – review & editing. **Marc W. Caffee:** Conceptualization, Methodology, Writing – review & editing. **James J. Camberato:** Methodology, Writing – review & editing. **Greg Michalski:** Methodology, Writing – review & editing.

Declaration of Competing Interest

The authors declare that they have no known competing financial interests or personal relationships that could have appeared to influence the work reported in this paper.

Acknowledgements

Funding for this research was provided by a grant from the Indiana Water Resources Research Center (IWRRC grant 105379). We thank Noah Stewart-Maddox and Zachary Meyers for assistance in collecting water samples, Greg Chmiel at the Purdue PRIME Lab for assistance with the ^{36}Cl analyses, and Darryl Granger for helpful discussions on the Teays River Valley. We thank Monica Lloyd of Compass Minerals and Scott Koefod of Cargill Deicing for samples of Silurian road salt. Randy Bayless (USGS Ohio-Kentucky-Indiana Water Science Center) provided helpful feedback on the hydrogeology of unconsolidated aquifers in northern Indiana. We thank Associate Editor Kenneth C. Carroll for assistance with the manuscript and Dioni I. Cendon and two anonymous reviewers for helpful comments on the manuscript. The data collected and interpreted for this study are available at: doi:10.4231/RNA2-WJ54.

References

Ahiablame, I., Chaubey, I., Engel, B., Cherkauer, K., Merwade, V., 2013. Estimation of annual baseflow at ungauged sites in Indiana USA. J. Hydrol. 476, 13–27. https://doi.org/10.1016/j.jhydrol.2012.10.002.

Austin, G.S., 1980. Potash in new Mexico. New Mex. Geol. 2 (1), 7–9.

Baker, D.B., Richards, R.P., Loftus, T.T., Kramer, J.W., 2004. A new flashiness index: characteristics and applications to Midwestern rivers and streams. J. Am. Water Resour. Assoc. (JAWRA), Paper No. 03095 503–522.

Bayless, E.R., Arihood, L.D., Reeves, H.W., Sperl, B.J.S., Qi, S.L., Stipe, V.E., Bunch, A.R., et al., 2017. Maps and grids of hydrogeologic information created from standardized water-well drillers' records of the glaciated United States. U.S.G.S. Scientific Investigations Report 2015-5105. https://doi.org/10.3133/sir20155105.

Brennan, S.T., Lowenstein, T.K., Cendón, D.I., 2013. The major-ion composition of Cenozoic seawater: the past 36 million years from fluid inclusions in marine halite. Am. J. Sci. 313, 713–775. https://doi.org/10.2475/08.2013.01.

Bruns, T.M., Steen, W.J., 2003. Hydrogeology of the Lafayette (Teays) Bedrock Valley System, north-central Indiana, State of Indiana, Department of Natural Resources, Division of Water. Water Resource Assessment 2003-7, 16 p.

Bugliosi, E.F., 1999. The Midwestern Basins and Arches Regional Aquifer System in parts of Indiana, Ohio, Michigan, and Illinois – Summary. U.S. Geological Survey, Professional Paper 1423-A, 60 p.

Burke, W.H., Denison, R.E., Hetherington, E.A., Koepnick, R.B., Nelson, H.F., Otto, J.B., 1982. Variation of seawater $^{87}Sr/^{86}Sr$ throughout Phanerozoic time. Geology 10, 516–519.

Buskirk, R.E., Malzone, J.M., Borowski, W.S., Cornelison, J., 2020. The impact of small-scale land cover and groundwater interactions on base flow solute and nutrient export in a small agricultural stream. Environ. Monit. Assess. 192 (574) https://doi.org/10.1007/s10661-020-08517-6.

Carlson, E.H., 1987. Celestite replacements of evaporites in the Salina Group. Sed. Geol. 54, 93–112.

Carlson, E.H., 1994. Geologic, fluid inclusion, and isotopic studies of the Findlay Arch District, northwestern Ohio. Econ. Geol. 89, 67–90.

Casey, G.D., 1996. Hydrogeologic framework of the Midwestern Basins and Arches Region in parts of Indiana, Ohio, Michigan, and Illinois. U.S. Geological Survey, Professional Paper 1423-B, 54 p.

Cendón, D.I., Ayora, C., Pueyo, J.J., Taberner, C., Blanc-Valleron, M.-M., 2008. The chemical and hydrological evolution of the Mulhouse potash basin (France): are "marine" ancient evaporites always representative of synchronous seawater chemistry? Chem. Geol. 252, 109–124. https://doi.org/10.1016/j.chemgeo.2008.01.019.

Clark, I., Fritz, P., 1997. Environmental Isotopes in Hydrogeology. CRC Press, Boca Raton.

Corcho Alvarado, J.A., Purtschert, R., Hinsby, K., Troldborg, L., Hofer, M., Kipfer, R., Aeschbach-Hertig, W., Synal, H.A., 2005. ^{36}Cl in modern groundwater dated by a multitracer approach ($^3H/^3He$, SF6, CFC-12 and ^{85}Kr): a case study in quaternary sand aquifers in the Odense Pilot River Basin, Denmark. *Appl. Geochem.* 20 (3), 599–609.

Craig, H., 1961. Isotopic variations in meteoric waters. Science 133, 1702–1703. https://doi.org/10.1126/science.133.3465.1702.

Culman, S., Fulford, A., Camberato, J., Steinke, K., 2020. Tri-State Fertilizer Recommendations, Bulletin 974. College of Food, Agricultural, and Environmental Sciences. The Ohio State University, Columbus, OH.

Daniels, D., Fritz, S., Leap, D., 1991. Estimating recharge rates through unsaturated glacial till by tritium tracing. Ground Water 29 (1), 26–34.

Davis, S.N., Whittemore, D.O., Fabryka-Martin, J., 1998. Uses of chloride/bromide ratios in studies of potable water. Ground Water 36 (2), 338–350.

Davis, S.N., Fabryka-Martin, J., Wolfsberg, L., Moysey, S., Shaver, S., Alexander Jr., E.C., Krothe, N., 2000. Chlorine-36 in ground water containing low chloride concentrations. Ground Water 38 (6), 912–921.

Davis, S.N., Moysey, S., Cecil, L.D., Zreda, M., 2003. Chlorine-36 in groundwater of the United States: empirical data. Hydrogeol. J. 11, 217–227. https://doi.org/10.1007/s10040-002-0232-6.

Doss, P.K., 1994. Middle Wabash River Basin. U.S. Geological Survey, Water-Resources Investigations. Report 92-4142, 16 p.
Dove, P.A., Czank, C.A., 1995. Crystal chemical controls on the dissolution kinetics of the isostructural sulfates: Celestite, anglesite, and barite. Geochim. Cosmochim. Acta 59 (10), I907–I1915.
Eberts, S.M., George, L.L., 2000. Regional ground-water flow and geochemistry in the Midwestern Basins and Arches Aquifer System in parts of Indiana, Ohio, Michigan, and Illinois. U.S. Geological Survey, Professional Paper 1423-C, 116 p.
Fausey, N., 2005. Drainage management for humid regions. Int. Agric. Eng. J. 14 (4), 209–214.
Feulner, A.J., Hubble, J.H., 1960. Occurrence of strontium in the surface and ground waters of Champaign County, Ohio. Econ. Geol. 55, 176–186.
Fidlar, M.M., 1943. The preglacial Teays Valley in Indiana. J. Geol. 51 (6), 411–418.
Foley, C.F., Bleuer, N.K., Leininger, R.K., Herring, W.C., 1972. Strontium and other notable chemical constituents of well-water of Allen County, Indiana. Proc. Indiana Acad. Sci. 82, 274–280.
Frankenberger, J., Kladivko, E., Sands, G., Jaynes, D.B., Fausey, N., Helmers, M.J., Cooke, R., Strock, J., Nelson, K., Brown, L.C., 2004. Drainage water management for the Midwest. *Agricultural and Biosystems Engineering Extension and Outreach Publications*. 1. http://lib.dr.iastate.edu/abe_eng_extensionpubs/1.
Freeze, R., Cherry, J., 1979. Groundwater. Prentice Hall Inc, Englewood Cliffs, NJ, p. 604.
Frisbee, M.D., Meyers, Z.P., Stewart-Maddox, N.S., Caffee, M.W., Bogeholz, P., Hughes, M.N., 2017. What is the source of baseflow in agriculturally-fragmented catchments? Complex groundwater/surface-water interactions in four tributary catchments of the Wabash River, Indiana, USA. Hydrol. Process. 39, 4019–4038. https://doi.org/10.1002/hyp.11345.
Frisbee, M.D., Meyers, Z.P., Miller, J.B., Box, C.L., Stewart-Maddox, N.S., Larson, E.B., Saksena, S., Dey, S., Frisbee, E.E., 2019. Processes leading to the activation (re-activation) of a paleokarst sinkhole and the subsequent drying of waterfalls in a small catchment located in northern Indiana, USA. *J. Cave Karst Stud.* 81 (2), 69–83. https://doi.org/10.4311/2017ES0116.
Fuzesy, A., 1982. Potash in Saskatchewan. Saskatchewan Geological Survey. Report 181, 48 p.
Gleason, C.L., Frisbee, M.D., Rademacher, L.K., Sada, D.W., Meyers, Z.P., Knott, J.R., Hedlund, B.P., 2020. Hydrogeology of desert springs in the Panamint Range, California, USA: Geologic controls on the geochemical kinetics, flowpaths, and mean residence times of springs. Hydrol. Process. 1–26 https://doi.org/10.1002/hyp.13776.
Gray, H.G., 2000. Physiographic divisions of Indiana. Indiana University, Indiana Geological Survey, Special Report 61, 26 p.
Hall, F.R., 1968. Base-flow recessions – A review. Water Resour. Res. 4 (5), 973–983.
Harkness, J.S., Sulkin, B., Vengosh, A., 2016. Evidence for coal ash ponds leaking in the southeastern United States. Environ. Sci. Technol. 50, 6583–6592. https://doi.org/10.1021/acs.est.6b01727.
Harrison, J.F., 2006. Softening up hard water. last accessed on 08 July 2020 Water Supply 48 (11), 172–173. https://www.pmengineer.com/articles/88588-water-treatment-softening-up-hard-water-br-joseph-f-harrison-p-e-cws-vi,.
Hawkesford, M., Horst, W., Kichey, T., Lambers, H., Schjoerring, J., Møller, I.S., White, P., 2012. Functions of macronutrients *in* Marschner's Mineral Nutrition of Higher Plants, Third Edition. Elsevier Ltd., London.
Hem, J.D., 1985. Study and interpretation of the chemical characteristics of natural water, 3rd ed., 2254. U.S. Geological Survey, Water-Supply Paper, p. 272.
Hogan, J.F., Blum, J.D., 2003. Tracing hydrologic flow paths in a small forested watershed using variations in $^{87}Sr/^{86}Sr$, [Ca]/[Sr], [Ba]/[Sr] and $\delta\ ^{18}O$. Water Resour. Res. 39 (10), 1282. https://doi.org/10.1029/2002WR001856.
Hogan, J.F., Phillips, F.M., Mills, S.K., Hendrickx, J.M.H., Ruiz, J., Chesley, J.T., Asmerom, Y., 2007. Geologic Origins of salinization in a semi-arid river: the role of sedimentary basin brines. Geology 35 (12), 1063–1066. https://doi.org/10.1130/G23976A.1.
Hoyer, B.E., Hallberg, G.R., 1991. Groundwater vulnerability regions of Iowa: Iowa Department of Natural Resources, Geological Survey Bureau Special Map Series II, 1 sheet.
ISWS, 2020. Lower and Middle Wabash watershed modeling. http://www.illinoisfloodmaps.org/wabashdiscovery.aspx, last accessed on 08 July 2020.
Kaushal, S.S., Likens, G.E., Pace, M.L., Utz, R.M., Haq, S., Gorman, J., Grese, M., 2018. Freshwater salinization syndrome on a continental scale. PNAS. https://doi.org/10.1073/pnas.1711234115.
Keith, B.D., 1985. Map of Indiana showing thickness, extent, and oil and gas fields of Trenton and Lexington Limestones. Indiana Geological Survey Miscellaneous Map 45.
Kell, S.R., Hodges, D.A., Tomastik, T., 2004. Spreading oil-field brine for dust and ice control in Ohio: A guidance for local authorities. U.S. Environmental Protection Agency, Project No. 90 (h) D-19.
Kladivko, E., 2020. Drainage for the long haul: Key takeaways from the SEPAC study. Purdue Agronomy Extension AY-396-W. https://ag.purdue.edu/agry/drainage/Pages/New-Summaries.aspx.
Kumar, P., Phong, V.V. Le, Papanicolaou, A.N. Thanos, Rhoads, B.L., Anders, A.M., Stumpf, A., Wilson, C. G., Bettis III, E.A., Blairi, N., Ward, A. S., Filley, T., Lin, H., Keefer, L., Keefer, D.A., Ling, Y-F, Musten, M., Royer, T.V., Foufoula-Georgiouo, E., Belmont, P., 2018. Critical transition in critical zone of intensively managed landscapes. *Anthropocene, 22*, 10-19, doi:10.1016/j.ancene.2018.04.002.
Luczaj, J., Masarik, K., 2015. Groundwater quantity and quality issues in a water-rich region: examples from Wisconsin, USA. Resources 4 (2), 323–357. https://doi.org/10.3390/resources4020323.
Maathuis, F., 2014. Sodium in plants: perception, signaling, and regulation of sodium fluxes. J. Exp. Bot. 65 (3), 849–858. https://doi.org/10.1093/jxb/ert326.
McLaughlin, P.I., Bancroft, A.M., Brett, C.E., Emsbo, P., 2018. The rise of pinnacle reefs: Islands of diversity in seas of despair. In: Florea, L.J. (Ed.), Ancient Oceans, Orogenic Uplifts, and Glacial Ice: Geologic Crossroads in America's Heartland, Field Guide 51. Geological Society of America, p. 433.
McNutt, R.H., Frape, S.K., Dollar, P., 1987. A strontium, oxygen, and hydrogen isotopic composition of brines, Michigan and Appalachian Basins, Ontario and Michigan. Appl. Geochem. 2, 495–505.
Melhorn, W.N., Kempton, J.P., 1991. Geology and hydrogeology of the Teays-Mahomet bedrock valley systems. Geol. Soc. Am. Spec. Pap. 258, 128 p.
Miller, S.A., Lyon, S.W., 2021. Tile drainage causes flashy streamflow response in Ohio watersheds. Hydrol. Process. 35, e14326 https://doi.org/10.1002/hyp.14326.
Munn, M.D., Frey, J.W., Tesoriero, A.J., Black, R.W., Duff, J.H., Lee, K., Maret, T.R., Mebane, C.A., Waite, I.R., Zelt, R.B., 2018. Understanding the influence of nutrients on stream ecosystems in agricultural landscapes. U.S. Geological Survey Circular 1437 80. https://doi.org/10.3133/cir1437.
Naylor, S., Letsinger, S., Ficklin, D., Ellett, K., Olyphant, G., 2016. A hydropedological approach to quantifying groundwater recharge in various glacial settings of the mid-continental USA. Hydrol. Process. 30 (10), 1594–1608. https://doi.org/10.1002/hyp.10718.
Panno, S.V., Hackley, K.C., Hwang, H.H., Greenberg, S.E., Krapac, I.G., Landsberger, S., O'Kelly, D.J., 2006. Characterization and identification of Na-Cl sources in ground water. Ground Water 44 (2), 176–187. https://doi.org/10.1111/j.1745-6584.2005.00127.x.
Parker, M.B., Gascho, G.J., Gaines, T.P., 1983. Chloride toxicity of soybeans grown on Atlantic Coast Flatwoods Soils. Agron. J. 75, 439–443.
Parker, M.B., Gaines, T.P., Gascho, G.J., 1985. Chloride effects on corn. Commun. Soil Sci. Plant Anal. 16, 1319–1333.
Phillips, F.M., 2000. Chlorine-36. In: Cook, P.G., Herczeg, A.L. (Eds.), Environmental Tracers in Subsurface Hydrology. Springer Science+Business Media, New York, pp. 299–348.
OH EPA, 2012. Fluoride in Ohio's ground water. Ohio EPA, Division of Drinking and Ground Waters Technical Series on Ground Water Quality, 10 p., https://epa.ohio.gov/Portals/28/documents/gwqcp/fluoride_ts.pdf, last accessed on 08 July 2020.
Phillips, F.M., 2013. Chlorine-36 dating of old groundwater, *in* Isotope Methods for Dating Old Groundwater, International Atomic Energy Agency, Vienna, Austria, Ch. 6, 125-152, ISBN 978–92–0–137210–9.
Pietz, R.I., Peterson, J.R., Lue-Hing, C., Welch, L.F., 1978. Variability in the concentration of twelve elements in corn grain. J. Environ. Qual. 7, 106–110.
Pinsak, A.P., Shaver, R.H., 1964. The Silurian formations of northern Indiana. Indiana Geol. Survey Bull. 32, 87.
Poff, N.L., Allan, J.D., Bain, M.B., Karr, J.R., Prestegaard, K.L., Richter, B.D., Sparks, R.E., Stromberg, J.C., 1987. The natural flow regime. Bioscience 47 (11), 769–784.
Pyron, M., Neumann, K., 2008. Hydrologic alterations in the Wabash River Watershed, USA. River Res. Appl. 24, 1175–1184. https://doi.org/10.1002/rra.1155.
Ruhl, L.S., Dwyer, G.S., Hsu-Kim, H., Hower, J.C., Vengosh, A., 2014. Boron and strontium isotopic characterization of coal combustion residuals: Validation of new environmental tracers. Environ. Sci. Technol. 48, 14790–14798. https://doi.org/10.1021/es503746v.
Sacks, L.A., Tihansky, A.B., 1996. Geochemical and isotopic composition of ground water, with emphasis on sources of sulfate, in the Upper Floridan Aquifer and Intermediate Aquifer System in Southwest Florida. U.S. Geol. Survey, Water-Resour. Invest. Rep. 96–4146, 59.
Schilling, K.E., 2005. Relation of baseflow to row crop intensity in Iowa. Agric. Ecosyst. Environ. 105, 433–438. https://doi.org/10.1016/j.agee.2004.02.008.
Schilling, K.E., Jindal, P., Basu, N.B., Helmers, M.J., 2012. Impact of artificial subsurface drainage on groundwater travel times and baseflow discharge in an agricultural watershed, Iowa (USA). Hydrol. Process. 26, 3092–3100. https://doi.org/10.1002/hyp.8337.
Schmidt, R. K., 2009. Bedrock aquifer systems of Adams County, Indiana, State of Indiana, Department of Natural Resources, Division of Water, Resource Assessment Section, 3 p.
Schnoebelen, D.J., Krothe, N.C., 1999. Reefs and nonreefs - a comparison of hydrogeology and geochemistry, northwestern Indiana. Ground Water 37 (2), 194.
Searcy, J.K., 1959. Flow-Duration Curves, USGS Manual of Hydrology: Part 2. Low-Flow Techniques, Water- Supply Paper 1542-A, https://pubs.er.usgs.gov/publication/wsp1542A.
Sharma, P., Bourgeois, M., Elmore, D., Granger, D., Lipschutz, M.E., Ma, X., Miller, T., Mueller, K., Rickey, F., Simms, P., Vogt, S., 2000. PRIME lab AMS performance, upgrades and research applications. Nucl. Instrum. Methods Phys. Res. B 172, 112–123.
Shaw, G.D., Conklin, M.H., Nimz, G.J., Liu, F., 2014. Ground water and surface water flow to the Merced River, Yosemite Valley, California: ^{36}Cl and Cl- evidence. Water Resour. Res. 50, 1943–1959. https://doi.org/10.1002/2013WR014222.
Sherman, L.S., Blum, J.D., Dvonch, J.T., Gratz, L.E., Landis, M.S., 2015. The use of Pb, Sr, and Hg isotopes in Great Lakes precipitation as a tool for pollution source attribution. Sci. Total Environ. 502, 362–374. https://doi.org/10.1016/j.scitotenv.2014.09.034.
Short, M.A., de Caritat, P., McPhail, D.C., 2017. Continental-scale variation in chloride/bromide ratios of wet deposition. Sci. Total Environ. 574, 1533–1543. https://doi.org/10.1016/j.scitotenv.2016.08.161.
Simsiman, G.V., Chesters, G., Andren, A.W., 1987. Effect of ash disposal ponds on groundwater quality at a coal-fired power plant. Wat. Res. 21 (4), 417–426.

Skaggs, R.W., Brevé, M.A., Gilliam, J.W., 1994. Hydrologic and water quality impacts of agricultural drainage. Crit. Rev. Environ. Sci. Technol. 24 (1), 1–32. https://doi.org/10.1080/10643389409388459.

Skaggs, R.W., Youssef, M.A., Gilliam, J.W., Evans, R.O., 2010. Effect of controlled drainage on water and nitrogen balances in drained lands. Trans. ASABE 53 (6), 1843–1850.

Sloan, B.P., Basu, N.B., Mantilla, R., 2016. Hydrologic impacts of subsurface drainage at the field scale: Climate, landscape and anthropogenic controls. Agric. Water Manag. 165, 1–10. https://doi.org/10.1016/j.agwat.2015.10.008.

Steeg, K.V., 1946. The Teays River. Ohio J. Sci. XLVI (6), 11.

Tesoriero, A.J., Duff, J.H., Saad, D.A., Spahr, N.E., Wolock, D.M., 2013. Vulnerability of streams to legacy nitrate sources. Environ. Sci. Technol. 47, 3623–3629. https://doi.org/10.1021/es305026x.

Tosaki, Y., Tase, N., Sasa, K., Takahashi, T., Nagashima, Y., 2011. Estimation of groundwater residence time using the ^{36}Cl bomb pulse. Ground Water 49 (6), 591–902. https://doi.org/10.1111/j.1745-6584.2010.00795.x.

Vengosh, A., Pankratov, I., 1998. Chloride/bromide and chloride/fluoride ratios of domestic sewage effluents and associated contaminated ground water. Ground Water 36 (5), 815–824.

Vengosh, A., 2014. Salinization and Saline Environments *in* Treatise on Geochemistry 2nd Edition, Elsevier, Amsterdam, Netherlands, 9144 pp, doi:10.1016/B978-0-08-095975-7.00909-8.

Warix, S.R., Rademacher, L.K., Meyers, Z.P., Frisbee, M.D., 2020. Groundwater geochemistry and flow in the Spring Mountains, NV: implications for the Death Valley Regional Flow System. J. Hydrol. 580, 124313 https://doi.org/10.1016/j.jhydrol.2019.124313.

Warren, J.K., 2016. Evaporites: A Geological Compendium, 2nd ed. Springer International Publishing. https://doi.org/10.1007/978-3-319-13512-0.

Welp-Smith, L., Meyer, A.L., Sparks, J., 2020. Precipitation stable isotopes from West Lafayette, IN, collection from Sep 8, 2015 to Jun 21, 2018. Purdue Univ. Res. Repository. https://doi.org/10.4231/ZYS8-CW17.

Wiener, M.J., Jafvert, C.T., Nies, L.F., 2016. The assessment of water use and reuse through reported data: A US case study. Sci. Total Environ. 539, 70–77. https://doi.org/10.1016/j.scitotenv.2015.08.114.

Wilson, C.G., Abban, B., Keefer, L.L., Wacha, K., Dermisis, D., Giannopoulos, C., Zhou, S., Goodwell, A.E., Woo, D.K., Yan, Q., Ghadiri, M., Stumpf, A., Pitcel, M., Lin, Y.-F., Marini, L., Storsved, B., Goff, K., Vogelgsang, J., Dere, A., Schilling, K.E., Muste, M., Blair, N.E., Rhoads, B., Bettis, A., Pai, H., Kratt, C., Sladek, C., Wing, M., Selker, J., Tyler, S., Lin, H., Kumar, P., Papanicolaou, A.N., 2018. The Intensively Managed Landscape Critical Zone Observatory: a scientific testbed for understanding critical zone processes in agroecosystems. Vadose Zone J. 17, 180088 https://doi.org/10.2136/vzj2018.04.0088.

Yaeger, M.A., Sivapalan, M., McIsaac, G.F., Cai, X., 2013. Comparative analysis of hydrologic signatures in two agricultural watersheds in east-central Illinois: legacies of the past to inform the future. Hydrol. Earth Syst. Sci. 17, 4607–4623. https://doi.org/10.5194/hess-17-4607-2013.

Yang, J., Blanchar, R.W., 1993. Differentiating chloride susceptibility in soybean cultivars. Agron. J. 85, 880–885.

Zhang, Y.-K., Schilling, K.E., 2006. Increasing streamflow and baseflow in Mississippi River since the 1940s: effect of land use change. J. Hydrol. 324, 412–422. https://doi.org/10.1016/j.jhydrol.2005.09.033.